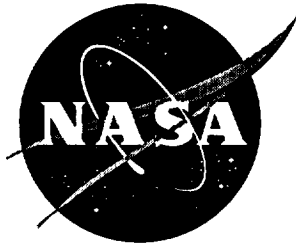NASA Technical Memorandum 110267

Correlation of Structural Analysis and Test Results for the McDonnell Douglas Stitched/RFI All-Composite Wing Stub Box

John T. Wang
Langley Research Center, Hampton, Virginia

Dawn C. Jegley
Langley Research Center, Hampton, Virginia

Harold G. Bush
Langley Research Center, Hampton, Virginia

Stephen C. Hinrichs
McDonnell Douglas Aerospace, Long Beach, California

July 1996

CORRELATION OF STRUCTURAL ANALYSIS AND TEST RESULTS FOR THE McDONNELL DOUGLAS STITCHED/RFI ALL-COMPOSITE WING STUB BOX

John T. Wang, Dawn C. Jegley, and Harold G. Bush
NASA Langley Research Center
Hampton, VA

and

Stephen C. Hinrichs
McDonnell Douglas Aerospace
Long Beach, CA

Abstract

The analytical and experimental results from a study of an all-composite wing stub box are presented in this paper. The wing stub box, which is representative of an inboard portion of a commercial transport high-aspect-ratio wing, was fabricated from stitched graphite-epoxy material with a Resin Film Infusion manufacturing process. The wing stub box was designed and constructed by the McDonnell Douglas Aerospace Company as part of the NASA Advanced Composites Technology program. The test article contained metallic load-introduction structures on the inboard and outboard ends of the graphite-epoxy wing stub box. The root end of the inboard load introduction structure was attached to a vertical reaction structure, and an upward load was applied to the outermost tip of the outboard load introduction structure to induce bending of the wing stub box. A finite element model was created in which the center portion of the wing-stub-box upper cover panel was modeled with a refined mesh. The refined mesh was required to represent properly the geometrically nonlinear structural behavior of the upper cover panel and to predict accurately the strains in the stringer webs of the stiffened upper cover panel. The analytical and experimental results for deflections and strains are in good agreement.

Introduction

The objective of this paper is to present the correlation between the analytical and experimental results for a full-scale graphite-epoxy wing stub box loaded in bending. The wing stub box represents the inboard portion of a high-aspect-ratio wing box for a civil-transport-aircraft. This wing box was designed and manufactured by the McDonnell Douglas Aerospace (MDA) Company under the NASA Advanced Composites Technology (ACT) Program. The wing stub box was fabricated using an innovative stitched/RFI (Resin Film Infusion) manufacturing process which has the potential for reducing manufacturing cost and producing damage-tolerant

1

composite primary aircraft structure. This wing stub box was subjected to a series of tests at the NASA Langley Research Center Structural Mechanics Test Laboratory. In the final test, the wing stub box was loaded to failure after being inflicted with a 100 ft-lb impact damage at a critical location. The final failure load (154 kips) is approximately 93% of the Design Ultimate Load (DUL) of 166 kips.

Finite element analysis results obtained prior to testing, (as presented in references 1 and 2), indicated that the wide bays outboard of the access door in the upper cover panel would not deform nonlinearly until loading approached the DUL. However, in the test of the wing stub box, documented in reference 3, large deformations occurred in this region at a load of approximately 130 kips, which is significantly less than DUL. Following the test, a more refined global finite element model of the wing stub box was developed in which a finer mesh was used for the wide bays to better account for their nonlinear behavior.

In addition to the refined global analysis, a local analysis that was presented in reference 4 and conducted prior to testing in order to study the splice joint between the stub box and the wing-tip extension structure was re-examined to help determine why measured strains were substantially greater than predicted. The abrupt termination of the stringers at the splice between the stub box and the wing-tip extension structure causes stress concentrations in the skin of the upper cover panel. Strain gages, located on the interior surface of the upper-cover-panel skin and at the base of three stringer webs, recorded strains up to twice the allowable strain for the skin material. In the pre-test local finite element analysis presented in reference 4, the predicted strain at the base of one of these stringers was examined and was predicted to be less than half of the strain that was recorded. Hence, post-test analytical study was conducted using a refined local model to help identify the difference between test data and analytical results.

The correlation between the experimental data and the results of the global and local analyses using the more refined models are presented in this paper. Analytical and experimental results are used to help understand the failure mechanisms of the composite wing stub box. Lessons learned from this study are also presented which are valuable for the design and analysis of future full-scale composite wing structures.

Wing-Stub-Box Test Article

The wing-stub-box test article consists of an inboard metallic load-transition structure at the wing root, the composite wing stub box, and an outboard metallic extension structure from the

composite wing stub box out to the wing tip. A photograph of the test article in the NASA
Langley Research Center Structural Mechanics Test Laboratory is shown in figure 1. As shown
in figure 2, the composite wing stub box is approximately twelve feet long and eight feet wide.
The maximum box depth, at the root of the composite wing stub box, is approximately 2.3 feet.
The composite wing stub box weighs approximately 1,200 lb. The load-transition structure and
the wing-tip extension structure are metallic end fixtures required for appropriate load
introduction into the composite wing stub box during the test. The load-transition structure is
located inboard of the composite wing stub box (between the composite wing stub box and the
vertical reaction structure at the wing-stub-box root). The wing-tip extension structure is located
outboard of the composite wing stub box. The load-transition structure is mounted to a steel and
concrete vertical reaction structure resulting in a near-clamped end condition. The entire
structure, including the composite wing stub box and the metallic structures, is approximately 25
feet long and weighs approximately 7,600 lb. Further details of the geometry of the structure are
presented in reference 5.

The composite wing stub box was fabricated from Hercules, Inc. AS4/3501-6 and IM7/3501-6
graphite-epoxy materials which were stitched together using E. I. DuPont de Nemours, Inc.
Kevlar thread. IM7 graphite fibers were used only for the 0 degree fibers in the lower cover
panel skin. The composite skin and stiffeners were composed of layers of the graphite material
forms prekitted in nine-ply stacks that have a $[45/-45/0_2/90/0_2/-45/45]_T$ stacking sequence. Each
nine-ply stack was approximately 0.058 inches thick after curing. Several nine-ply stacks of the
prekitted material were used to build up the desired thickness at each location. The fabrication of
this composite wing stub box using an innovative RFI process is described in reference 6.

As shown in figures 3 and 4, the composite wing stub box consists of ribs, spars, and upper and
lower cover panels (each of which has stringers and intercostals stitched to the skin). The skin
of the upper and lower cover panels range in thickness from approximately 0.29 to 0.90 inches.
The upper cover panel has ten stringers oriented along the length of the wing box, as shown in
figure 3. The lower cover panel has eleven stringers oriented along the length of the wing box,
and is similar to the upper cover panel except that it has no access-door cutout. The skin in the
upper cover panel consists of five to ten of the nine-ply prekitted stacks, depending upon the
location on the wing, as shown in figure 5. The skin in the lower cover panel contains from six
to fifteen of the nine-ply prekitted stacks, depending upon the location on the wing.

The stringer webs were made from eight nine-ply prekitted stacks (except at stiffener runouts
where the stringer webs are tapered and the number of stacks is gradually reduced from eight to

3

two). At the stringer runout, a stringer is terminated and the tapered stringer web provides a mechanism for smoothly transferring the load from the stringer to the skin. Stringers in the upper cover panel were spaced uniformly seven inches apart except for the bay which contains the access door. The stringers on either side of the access-door bay and two adjacent outboard wide bays are 18 inches apart. The stringer webs are approximately 2.3 inches high and 0.464 inches thick. Each stringer flange on either side of the web is 1.12 inches wide and the flange is half the thickness of the web. Since the cover panels were stitched and fabricated using the RFI process, no mechanical fasteners were required. However, at the stiffener runout locations, fasteners were installed to prevent skin-stiffener debonding at these locations. One composite blade stiffener and two metal angles, oriented parallel to the ribs, were added to the wide bays of the upper cover panel to prevent the skin from buckling prematurely.

The ribs and spars were made of conventional AS4/3501-6 graphite-epoxy preimpregnated fabric and tape materials, respectively. The ribs and spars were stiffened with blade stiffeners to prevent buckling as shown in figure 4. The ribs were connected to the cover panels at intercostals (see figure 3) which were attached to the skins. The intercostals are approximately 2.3 inches tall and 0.116 inches thick. Spar webs have a constant thickness of 0.31 inches and rib webs have a thickness of 0.15 inches.

This wing-stub-box test article was subjected a series of tests as documented in reference 3. The wing stub box was loaded to failure in the final test. Before the final test, a 100 ft-lb impact damage was inflicted at the stringer Runout 2 (see figure 3). The impact dent depth is 0.0134 inches which is invisible. The damage area from nondestructive testing is approximately 4.0 inches long and 3.0 inches wide. A recording from a video camera indicated that the failure was initiated from the impact site and propagated across the wing-stub-box upper cover panel (see figure 3).

Material Properties and Allowables

The material properties used in the analyses for the stitched AS4/3501-6 prekitted stacks of material in the upper cover panel, the stitched AS4/IM7/3501-6 prekitted stacks of material in the lower cover panel skin, the AS4/3501-6 fabric material in the ribs, and the AS4/3501-6 tape material in the spars are shown in table 1. The material properties used for the steel and aluminum load-introduction structures are also given in table 1. All material properties used in this study were provided by MDA.

In the upper and lower cover panels, the x-direction, which is parallel to the rear spar, is coincident with the 0-degree fiber direction. In the ribs and spars, the x-direction is coincident with the 0-degree fiber direction which is perpendicular to the plane of the upper cover panel.

The axial compressive strain allowable and the shear strain allowable for the undamaged upper cover panel is 0.00933 and 0.0126, respectively. These allowables were established by MDA.

Finite Element Models

Since the initial global and local finite element analyses, described in references 2 and 4, respectively, did not accurately predict the behavior of the test article at the center portion of the upper cover panel or at the splice joint between the composite stub box and the metallic extension box, refined models were created to improve the accuracy of analytical predictions.

Refined Global Model

The primary differences between the initial and refined global models are the mesh density of the upper-cover-panel skin outboard of the access door and the modeling of some blade stiffeners as plate elements rather than the beam elements used initially. The finite element mesh of the upper-cover-panel skin in the initial and refined models is shown in figures 6 and 7, respectively. More details of the mesh refinement are shown in figure 8. The number of quadrilateral, triangular, and beam elements used in the initial and in the refined global models are shown in table 2. The initial model contains 5,266 grid points and the refined model contains 9,557 grid points.

Refined Local Splice Model

The location of the splice is shown in figure 3. As shown in figure 9, metal splice plates were used in this region to join the composite stub box to the outboard extension box and a local splice model is required to represent the complex structural details. The primary difference between the initial and refined local splice models is the meshing in the upper-cover-panel skin at the base of the terminated stiffener. The upper-cover-panel skin in the initial and refined local models is shown in figure 9. In refining the mesh of the initial model, the element size in the region of the skin at the base of the stringer web was reduced from 0.4 inches to 0.05 inches and the number of elements was increased from 2,201 to 2,301. The initial model contains 2,544 grid points and the refined model contains 2,667 grid points.

5

Analysis

The MSC/NASTRAN finite element code (reference 7), Version 68 was used to perform buckling and nonlinear analyses of the initial model before testing and to perform analyses of the refined global model after testing. Solution sequences 105 and 106 were used to conduct buckling and geometrically nonlinear analyses, respectively. PATRAN (reference 8) was used to create the refined global model and to postprocess the analytical results. The STAGS finite element code (reference 9) was used to conduct the nonlinear analyses of the initial and refined local splice joint models.

Buckling Results

Buckling analyses were performed using the initial and refined global models. For the mode shape shown in figure 10, the analysis using the initial model predicted a buckling load of 185 kips while the analysis using the refined model predicted a buckling load of 160.7 kips. The buckling load predicted by the refined global model is approximately 15% less than that predicted by the initial model.

Correlation of Analysis and Test Results

Correlation between results of the nonlinear analyses and test data is presented. A comparison using the analysis results from the initial global is presented first to show that the initial global model did not predict the nonlinear deformation accurately. All succeeding results are based on the analysis using the refined global model, except for the results at the compression splice, which are based on the initial and refined local splice models. Although a series of tests were conducted on the wing stub box (reference 3), all experimental results presented herein are from the final test when the wing stub box was loaded to failure. The locations of all strain gages discussed in this section are shown in figure 3.

Results Based on the Initial Global Model and Experiment

The deformed shape of the test article predicted by the initial global model at the test failure load of 154 kips is shown in figure 6. The region bounded by stringers on either side of the access-door cutout displayed some geometrically nonlinear deformations in the initial analysis.

6

However, during testing, back-to-back strain gages in the center of that region, strain gages 63 and 64 in figure 6, recorded significantly higher strains than predicted by the nonlinear analysis when the applied load exceeded 130 kips, as shown in figure 11. This discrepancy indicates that the initial model could not predict the nonlinear deformation and high strains in the large bay region. Also, the initial model shown in figure 6 has four elements across the skin bay, which may be insufficient to represent the nonlinear behavior of the stub box.

Results from the Refined Global Model and the Experiment

Displacements and strains obtained from testing and from the analysis using the refined global model are presented in this section.

Correlation of displacement results - Analytical predictions and experimental results for the vertical displacements, measured by Direct Current Differential Transformers (DCDT's), at six locations on the stub box and at the wing tip are shown in figures 12-14. These figures show the variation of vertical displacements with the applied load at the wing tip. Rigid body motions of the load-transition structure relative to the vertical reaction structure were removed from the measured results to obtain the results presented in these figures. At the wing tip, the difference between the experimental and the analytical results is approximately 6 %, as shown in figure 12. Measurements at three locations along the rear spar are shown in figure 13, and measurements at three locations along the front spar are shown in figure 14. The average of errors between the analytical results and the experimental results at these six locations is less than 6%.

The predicted deformed shape of the composite stub box subjected to the test failure load of 154 kips is shown in figure 15. The relatively large out-of-plane deformation in the upper cover panel outboard from the access door is caused by the lack of longitudinal support in this region. Out-of-plane displacements were measured at six locations on the upper cover panel. DCDTs 7, 8 and 9 are located along line A-A (shown in the insert of figure 16) at 18, 33 and 63 inches from the access-door cutout, respectively. DCDTs 10, 11 and 12 are located along line B-B (shown in the insert of figure 16) at 18, 33 and 63 inches from the access-door cutout, respectively. Lines A-A and B-B are parallel to the rear spar. Line B-B is located 15.875 inches aft of line A-A. Line B-B is sufficiently removed from the nonlinearly deformed skin bays outboard of the access door that it can be considered as a far field location; thus, measurements along line B-B are assumed to represent the global behavior of the stub box. Measurements along line A-A represent a combination of the global behavior of the stub box and the large local deformations of the skin. The difference in these measurements provides a good measure of the nonlinearity

7

developing in the wide bays outboard of the access door. The analytical and experimental results of the relative out-of-plane displacements (e.g., displacement at DCDT 11 subtracted from displacement at DCDT 8) are shown in figure 16.

The experimental and analytical results correlate well for the locations 18 and 33 inches from the access-door cutout. However, the agreement between experimental and analytical results is not acceptable for the location 63 inches from the access-door cutout. An explanation of this discrepancy is presented in a subsequent section about failure.

Correlation of strain results - A contour plot of the predicted axial strains on the outer surface of the upper-cover-panel skin at an applied load of 154 kips is shown in figure 17. The axial x-direction is parallel to the rear edge of the panel. Analytical and experimental strains for strain gages 17, 20, 74, 84 and 602 are plotted in figures 18 through 22. These strain gages are located sufficiently far from the access-door cutout and the nonlinearly deformed region to be considered as far field results. In each of the figures, the hatched region in the sketch of the wing stub box is the mesh refinement region. These correlation plots indicate that the far field strains predicted by the analysis are quite accurate. High strains can be seen at the edge of the access-door cutout and in the region outboard of the access door where large nonlinear deformations occurred. Analytical and experimental strains at the strain gage locations in these regions and near the impact site are shown in figures 23-32.

Strain results on the external surface of the cover panel skin at the edge the access-door cutout, measured by strain gages 78 and 79, are shown in figure 23. Analytical and experimental results for these external strain gages indicate approximately linear behavior with no strain exceeding 0.0075. Moreover, the experimental results show that no failures occurred in the region of the access-door cutout.

Predicted and measured strain results for the first and second bays outboard of the access-door cutout of the upper cover panel are shown in figures 24 through 28. The first and second bays are 18 inches wide, and they deformed nonlinearly due to the lack of longitudinal stiffeners. Results for strain gages 67 and 68 on the upper-cover-panel skin in the first bay, immediately outboard from the access door, are shown in figure 24. Results for strain gages 613 and 614 on the external skin at the edge of this bay are shown in figure 25. Results for strain gages 63 and 64 on the upper-cover-panel skin in the second bay outboard of the access door are shown in figure 26. Results for strain gages 22-24 , 607 and 608 at the edge of this bay are shown in figures 27 and 28. Results for strain gages 22- 24 at the aft edge of the nonlinearly deformed

8

region are shown in figure 27, while results for strain gages 607 and 608 at the forward edge of the nonlinearly deformed region are shown in figure 28.

Good correlation was obtained between experimental and analytical results in the skin and on the stiffeners for the first and second bays outboard of the access door, as shown in figures 24 to 28. The refined analysis accurately predicts strains in these two bays of the nonlinearly deformed region while the initial model did not accurately predict the nonlinear response in this region.

Predicted and measured strain results for the third bay outboard of the access door of the upper cover panel are shown in figures 29 through 32. The third bay has two stringer runouts and is also in the mesh refinement region. Results for strain gages 49 and 50, located at the center of the third bay outboard of the stringer Runout 3 (see figure 3), are shown in figure 29. Strain results for gages 51 and 54, located at the forward edge of the third bay inboard of the stringer Runout 2, are shown in figure 30. The correlation between experimental and analytical strain results shown in figures 29 and 30 is good.

Strain results for internal strain gages 55, 56 and 57 and external strain gage 58 near stringer Runout 3 are shown in figure 31. Strain gages 55 and 56 are located on the stringer flange. Good agreement can be seen between the analytical and experimental results for the stringer-flange strain gages for loads less than approximately 130 kips. The erratic strains recorded at loads above 130 kips by strain gages 55 and 56 indicate that a local failure has just occurred at this load level. The analysis predicts significantly more strain than was recorded by strain gage 57 on the intercostal flange, and by strain gage 58 on the external surface of the skin. The correct trend is predicted on the external surface, including the nonlinear behavior. However, for loads below 130 kips, the strain recorded by gage 57 on the intercostal flange is linear, but it is much less than the predicted strain. The discrepancy between analytical and experimental strain results from gage 57 may be attributed to that this gage was placed right next to edge of a intercostal flange (see insert in figure 31), and the discontinuity of thickness may cause the inaccurate strain predication at this location.

Strain results for gages 43 through 46 on the upper cover panel in the stringer Runout 2 region are shown in figure 32. Poor correlation for strain gages 44 and 45 is very likely due to this location being subjected to a 100 ft-lb impact damage to the external skin prior to the final test. Strain gages 44 and 45 are located on interior flanges less then 0.4 inches from the impact site. The data recorded for these two strain gages from this final test are not the same as in previous

9

tests (as described in reference 3 for these previous tests involving no impact damage at stringer Runout 2). Since the analysis does not consider damage in this region, correlation between the final test results and analytical results should not be expected for strain gages 44 and 45. Strain gages 43 and 46 are approximately one inch from the impact site, where little damage would be expected. For loads below 120 kips, linear behavior is observed for strain gage 43, which is mounted on the flange of the runout stringer, and the experimental and analytical data correlate well. At higher loads, some nonlinear behavior is observed in the experimental results and significant discontinuities in the data can be seen at loads of approximately 140 kips and 145 kips, indicating local failures and load redistribution. However, no such discontinuities can be seen in the external strain gage, gage 46. Further discussion of this apparent interior local failure is presented in a subsequent section on failures.

Results Based on the Local Splice Models and Experiment

Results of the pre-test finite element local analysis in the vicinity of strain gages 38 and 39 are presented in reference 4. The initial finite element model was refined by increasing the number of elements of the skin at the base of the terminated stringer web (see figure 9). Details of the analysis procedure, which were reported in reference 4, were not changed for the new analysis and are not repeated here.

Experimental data and analytical results for strain gages 38 and 39 are shown in figure 33. For loads less than 130 kips, the results from the refined analysis agree well with the test data and are approximately linear. This same strain was recorded during each of the four tests of the stub box. The sudden change in the slope of the load-strain curve of the test data at approximately 130 kips can be attributed to local failures elsewhere in the stub box since no failure was detected at this splice.

These results indicate that to represent the high strain concentration in the upper-cover-panel skin at the base of the stringer web, a very detailed model is needed in the small local region of high strains. However, surface strains well in excess of the allowable strains can be withstood in localized regions without failure when the structure is loaded primarily in compression. The structure has a very small local region of stress concentration (0.3 inches in this case), and other load paths are provided by heavily stiffened surrounding structures.

10

Failures and Load Redistribution

Test results indicate that catastrophic failure of the stub box occurred when the upper-cover-panel skin failed through the impact site at stringer Runout 2. Post-test evaluation of the test article revealed local failures in both stringer Runouts 2 and 3 (see figure 8 for locations). These failures occurred in the thinnest portion of the web and flange of the stringer runout. The failure at stringer Runout 3 is shown in figure 34. While the stringer separated from the skin, no skin failure is evident at stringer Runout 3. Displacement and strain gage data at stringer Runout 3 indicate that an initial failure may have occurred at a load of approximately 135 kips as evidenced by discontinuities in the readings of strain gage 55 which is on the stringer runout flange, as shown in figure 31. However, no measured axial strain in this region is greater than the allowable strain. Shear strain in the stringer runout web was not measured experimentally, but analytical results indicate the presence of high shear strains in the thinnest portion of the stringer runout web, at the failure location. A contour plot of the shear strain at the failure load in the stringer runout web is shown in figure 35. The analytical results indicate that the shear strain alone would have been enough to induce failure prior to the maximum load of 154 kips applied to the test article.

The behavior of stringer Runout 2 is similar to the behavior of stringer Runout 3. The present model, which does not account for the reduction of stiffness in the impact damage zone near stringer Runout 2, predicted that the maximum shear strain at the failure load in the stringer web at stringer Runout 2 is 0.01069 which is about 15% below the shear allowable. However, when other factors, such as the axial strain in the stringer web and the increase of stringer web load due to the reduction of load carrying capability of the impact damage zone, are taken into consideration, failure of the stringer web at the stringer Runout 2 is likely. Indeed, the discontinuity of strain results from strain gage 43 indicate that a local failure occurred at 140 to 145 kips (see figure 32). An analysis that assumed the stiffener web at stringer Runout 2 had failed predicted an increase in the skin axial stress resultant of about 3.6% in the stringer runout region. The catastrophic failure of the box involving the skin failure at stringer Runout 2 occurred at a load of 154 kips, thereby implying that the stringer runout web failure did not immediately propagate into the skin. The test of an intermediate wing box, which has the same stringer runout design as the stringer runouts in the stub box, resulted in the same failure mode, as described in reference 10. A video camera inside the intermediate wing box confirmed this analytically-based failure scenario. It recorded the failure progression at that stringer runout and the failure of the thin web and flange occurring well before the failure of the skin. Strain gage

11

behavior for the intermediate-wing-box stringer runout is similar to the strain gage behavior for the stub-box stringer runouts.

In order to determine whether the failure at stringer Runout 2 was activated prematurely by the large deformation in the upper-cover-panel skin and the failure in stringer Runout 3, axial stress resultants in the upper cover panel were computed by the analysis. Analytical results for axial stress resultants in the vicinity of stringer Runout 2 are presented in figures 36 through 38. The axial stress resultants, N_{xx}, for the elements in the thinnest section of the stringer runout flange, for the skin elements next to the intercostal flange, and for the elements in the intercostal flange are shown in the figures. Results for all of these elements indicate linear behavior for the complete load range. No evidence can be seen in these elements of any influence of the large nonlinear deformation elsewhere in the upper cover panel. Hence, the large nonlinear deformations in the upper cover panel appear to have no influence on the final failure.

Concluding Remarks

The correlation of the analytical and experimental results for the bending of an all-composite stitched/RFI wing stub box is documented in this paper. The wing stub box was designed and fabricated by the McDonnell Douglas Aerospace Company. Displacements and strains predicted by a geometrically nonlinear analysis using a refined finite element model are compared with the test results. Excellent agreement is found between analytical results and test data at most locations prior to failures in the structure.

A refined global model with a finer mesh in the large nonlinearly deformed region of the upper cover panel provided more accurate results than could be obtain with the initial model. A 15% reduction in buckling load and considerably larger nonlinear strains and displacements were predicted by the analysis using the refined model compared to results obtained using the initial model. The strains in the nonlinearly deformed region agree well with the test data. These results indicate that the initial model was too stiff to represent the nonlinear behavior of the wide bay region in the upper cover panel.

The upper cover panel of the stub box contains two critical stringer runouts. One of these runouts is located outboard from the access-door cutout in the nonlinearly deformed region. The other critical stringer runout is located near the front spar. Only the runout near the front spar was impact damaged. The analysis indicates that the high shear strains in both these stringer runout webs exceeded the material allowable and led to local stringer web

12

failures. These shear strains were not monitored during the tests. However, the erratic strains recorded by strain gages in the stringer runout regions indicate that these runouts failed prior to final catastrophic failure.

Based on analytical and experimental results, the sequence of events that led to the structural failure of the wing stub box included the onset of nonlinear deformations in the large skin bays outboard from the access-door cutout, followed by local stringer web and flange failure in the runout stringer in the nonlinearly deformed region. The skin at this runout stringer remained intact throughout the test. The next event was the failure of the web and flange of the impact-damaged runout stringer near the front spar. Finally, the catastrophic failure of the upper-cover-panel skin initiated from the impact site at the impact-damaged runout. The failure propagated across the entire upper cover panel. The analysis indicates that the nonlinear deformation of the wide bays and the failure of the first stringer runout did not significantly redistribute the load into the impact-damaged region.

Acknowledgment

References

1. Hinrichs, S. C., Jegley, D. C., and Wang, J. T., "Structural Analysis and Test of a Stitched Composite Wing Box," Presented in the *6th NASA/DoD Advanced Composite Technology Conference*, Anaheim, CA, August 7-11, 1995.
2. Wang, J. T., *Global and Local Stress Analyses of McDonnell Douglas Stitched/RFI Composite Wing Stub Box*, NASA TM-110171, December 1995.
3. Jegley, D. C. and Bush, H. G., *Test Documentation and Results of the Structural Tests on the All-Composite McDonnell Douglas Wing Stub Box*, NASA TM 110204, April 1996.
4. Jegley, D. C., *Analysis of Selected Compression Splice Joint Locations In A Graphite-Epoxy Transport Wing Stub Box*, NASA TM 110170, October 1995.
5. Markus, A. M., and Grossheim, B. G., "Manufacturing Development for Stitched/RFI Transport Wing Stub Box Structures," *Proceedings of the Fifth NASA/DoD Advanced Composites Technology Conference*, NASA CP 3294, pp. 773-786, May 1995.

6. Markus, A. M., Thrash, P., and Grossheim, B. G., "Manufacturing Development and Requirements for Stitched/RTM Wing Structure," *Proceedings of the Fourth NASA/DoD Advanced Composites Technology Conference*, NASA CP 3229, pp. 503-523, 1993.

7. Anon., MSC/NASTRAN Reference Manual, Version 68, The MacNeal-Schwendler Corporation, April 1994.

8. Anon., PATRAN Plus User Manual, Release 2.4, PDA Engineering, Publication Number 2191023, September 1989.

9. Brogan, F. A., Rankin, C. C., and Cabiness, H. D., *STAGS User Manual*, Lockheed Palo Alto Research Laboratory, LMSC Report P032594, 1994.

10. Hinrichs, S. C., *ICAPS Intermediate Wing Box Test Results*, McDonnell Douglas Aerospace Transport Aircraft-West Report Number MDC94K9115, May 1995.

Table 1. Material properties.

Property	Stitched AS4/3501-6	Stitched AS4/IM7/ 3501-6	AS4/3501-6 Fabric/Tape	Steel	Alumim
E_x	8.17 Msi	11.85 Msi	7.32/6.12Msi	29.0 Msi	10.0 Msi
E_y	4.46 Msi	4.55 Msi	7.32/6.12 Msi	29.0 Msi	10.0 Msi
G_{xy}	2.35 Msi	2.57 Msi	3.32/3.98 Msi	11.0 Msi	3.76 Msi
v_{xy}	0.459	0.409	0.357/0.459	0.32	0.33

Table 2. Element types and total number of elements for the initial model and the refined model.

Element Types (reference 7)	Initial Model	Refined Model
CQUAD4 (Quadrilaterial)	4,408	7,923
CTRIA3 (Triangular)	99	182
CBEAM (Beam)	2,050	1,968
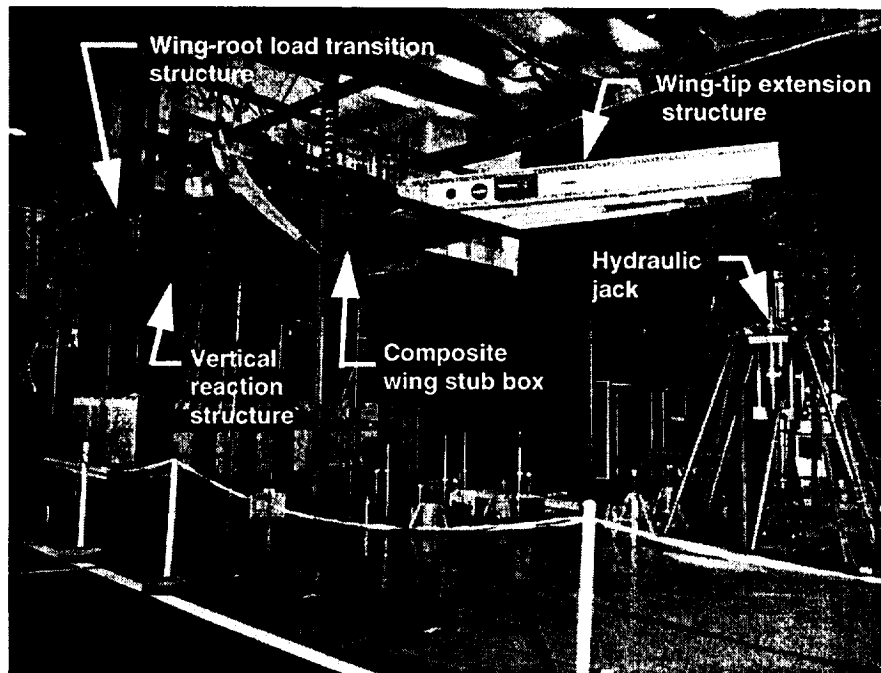
Figure 1. Wing-stub-box test article attached to the vertical reaction structure.
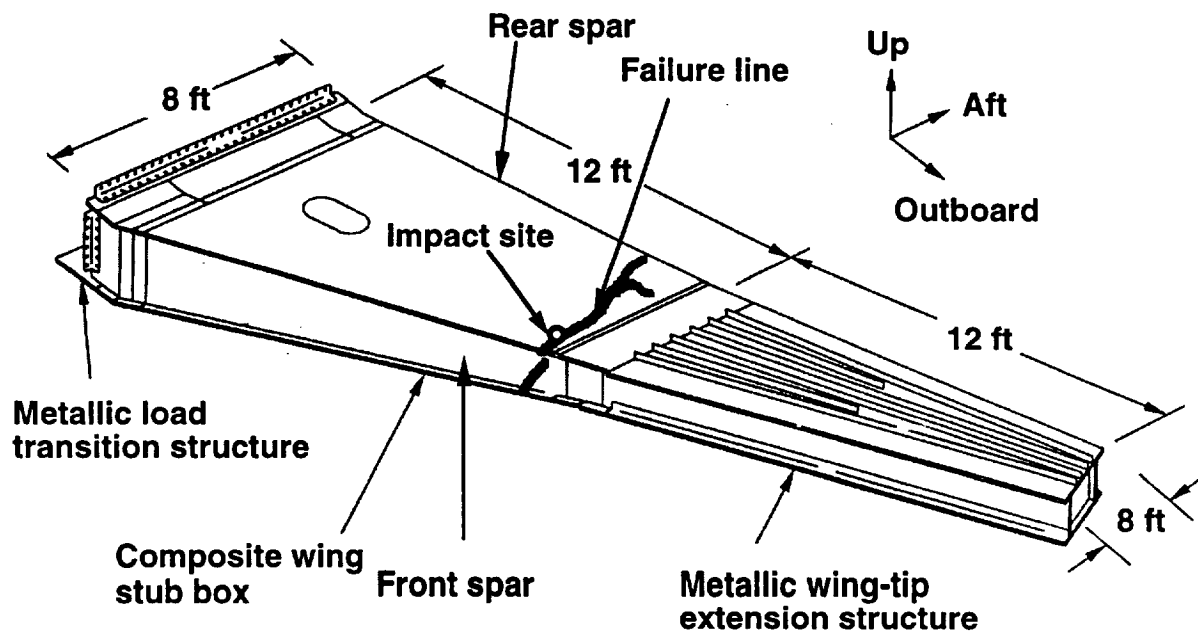
Figure 2. Dimensions of the wing-stub box test article.

15
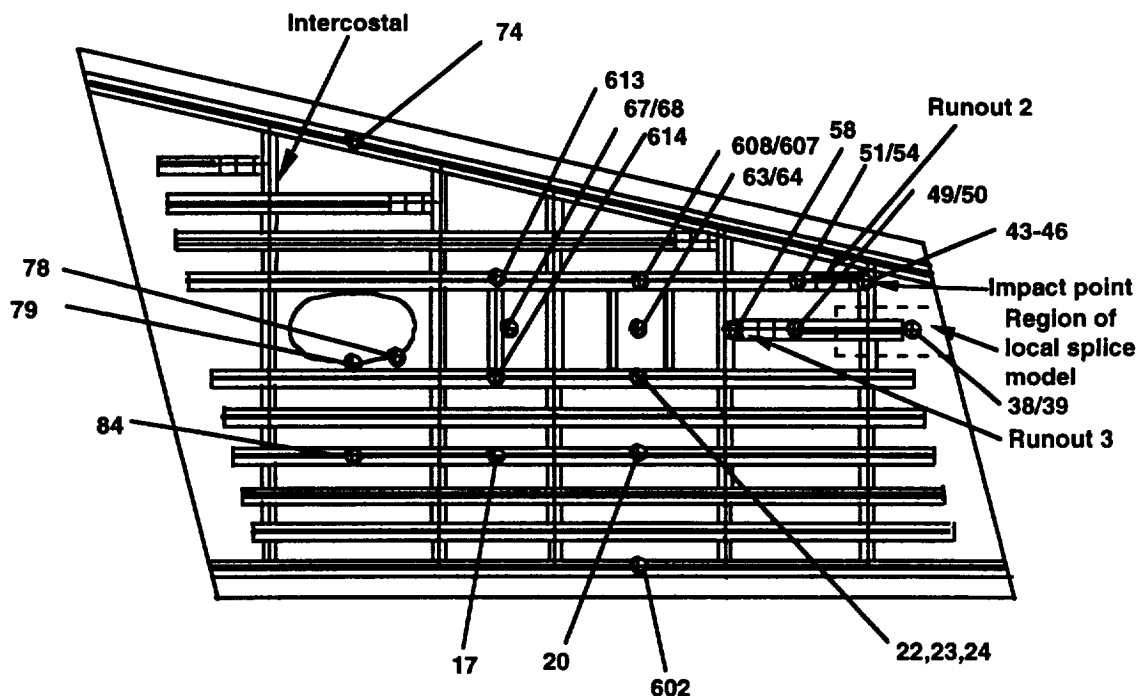
Figure 3. Upper cover and strain gage locations (the numbers on the figure identify specific strain gages).
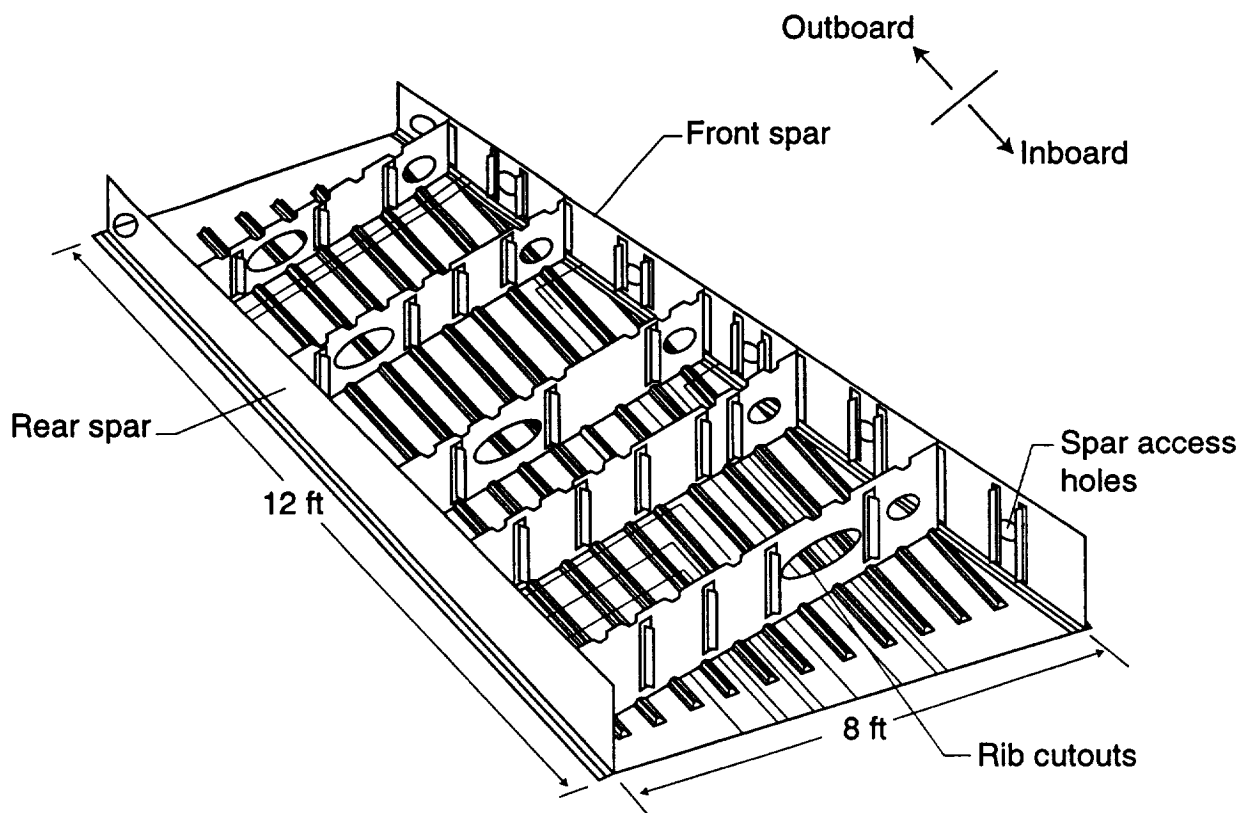
Figure 4. Interior of the composite stub box.

16
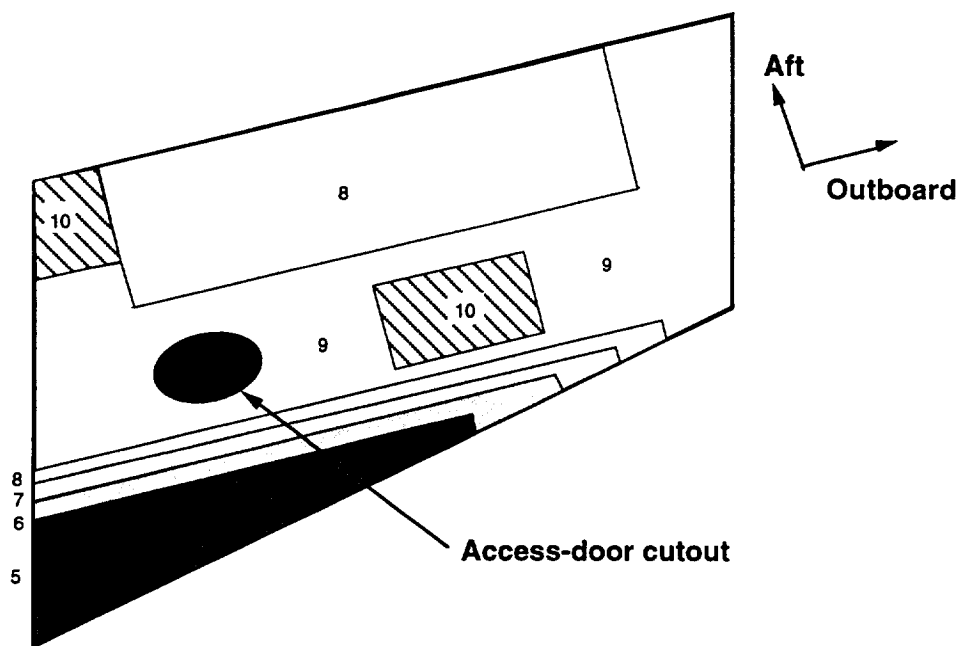
Figure 5. Stub box upper cover panel skin thickness distribution (the numbers on the figure represent the number of prekitted stacks of the graphite-epoxy material at a given location).
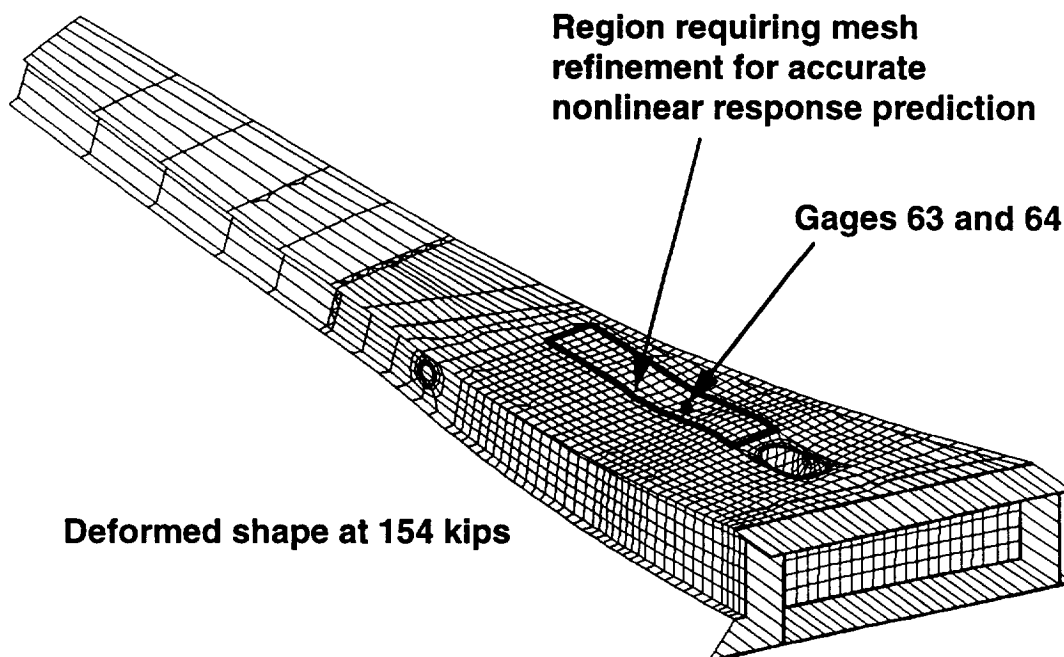
Figure 6. Finite element mesh of the original model and location of a region that requires mesh refinement for accurate nonlinear response prediction.

17
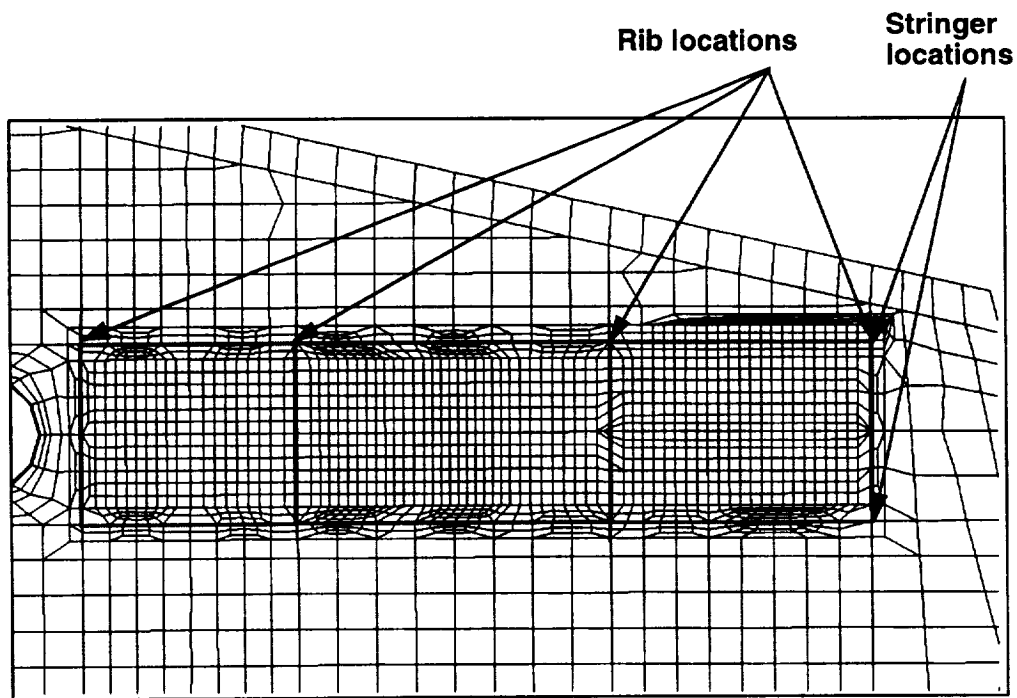
Figure 7. Refined mesh in three bays of the stub-box upper cover panel.
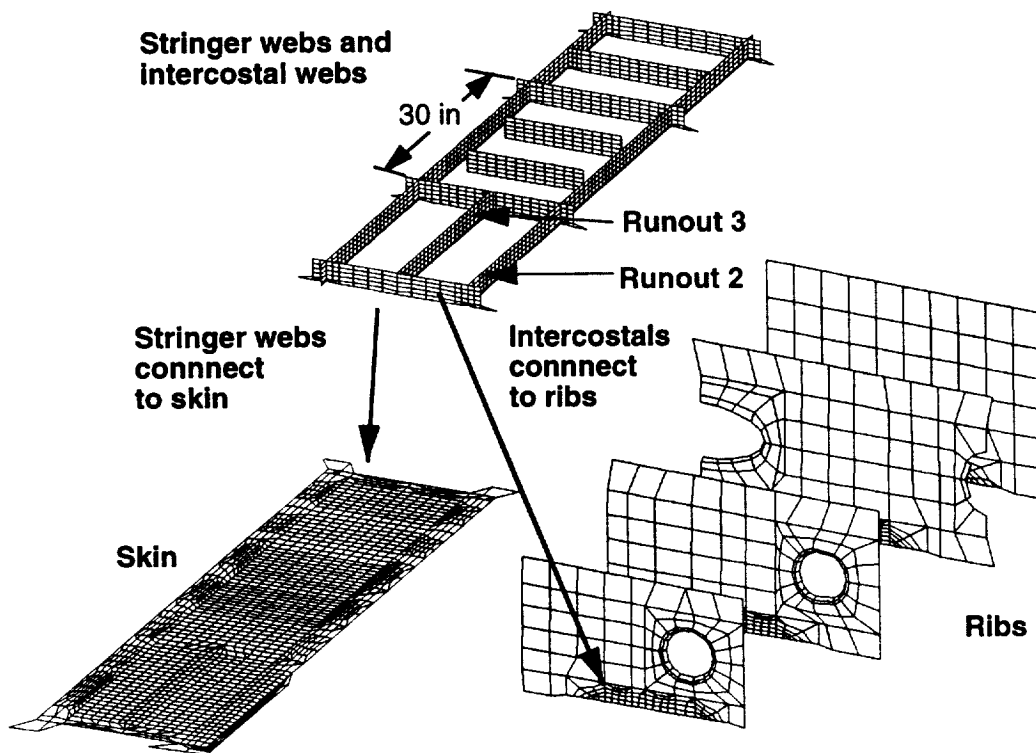
Figure 8. Refined finite element models for the skin, blade stiffeners, and intercoastals.
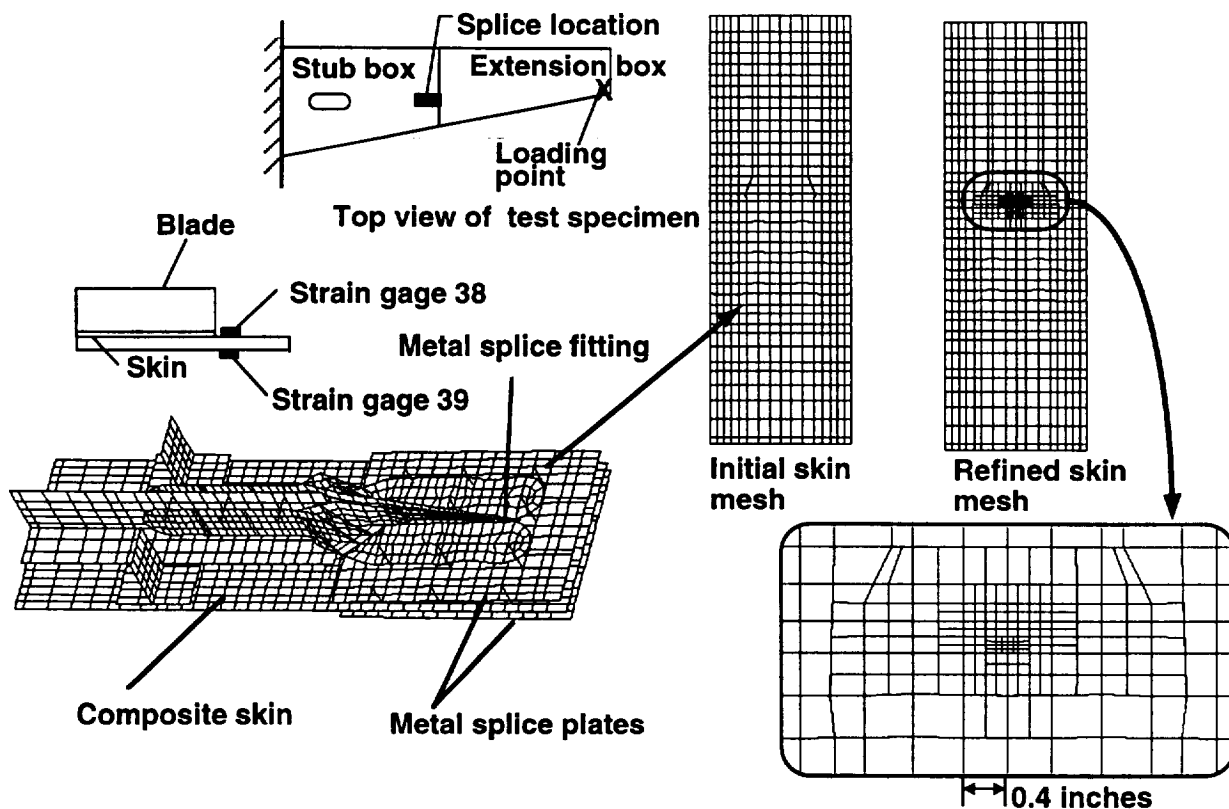
Figure 9. Compression splice and skin models.

Buckling load = 160.7 kips
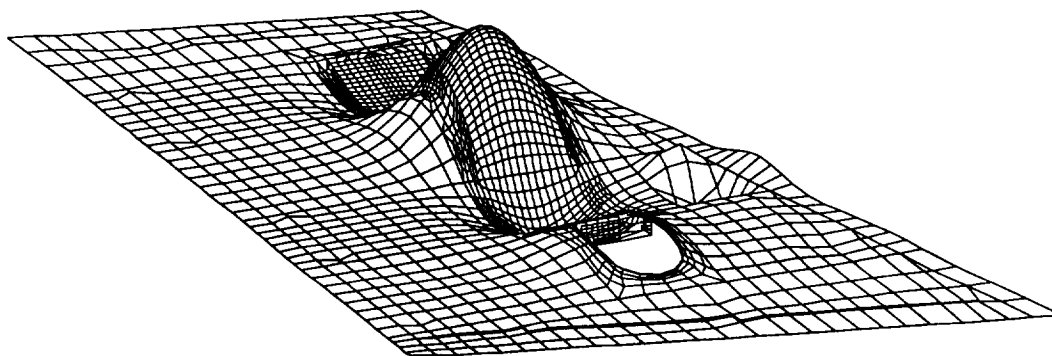
Figure 10. Buckling mode for the refined model.
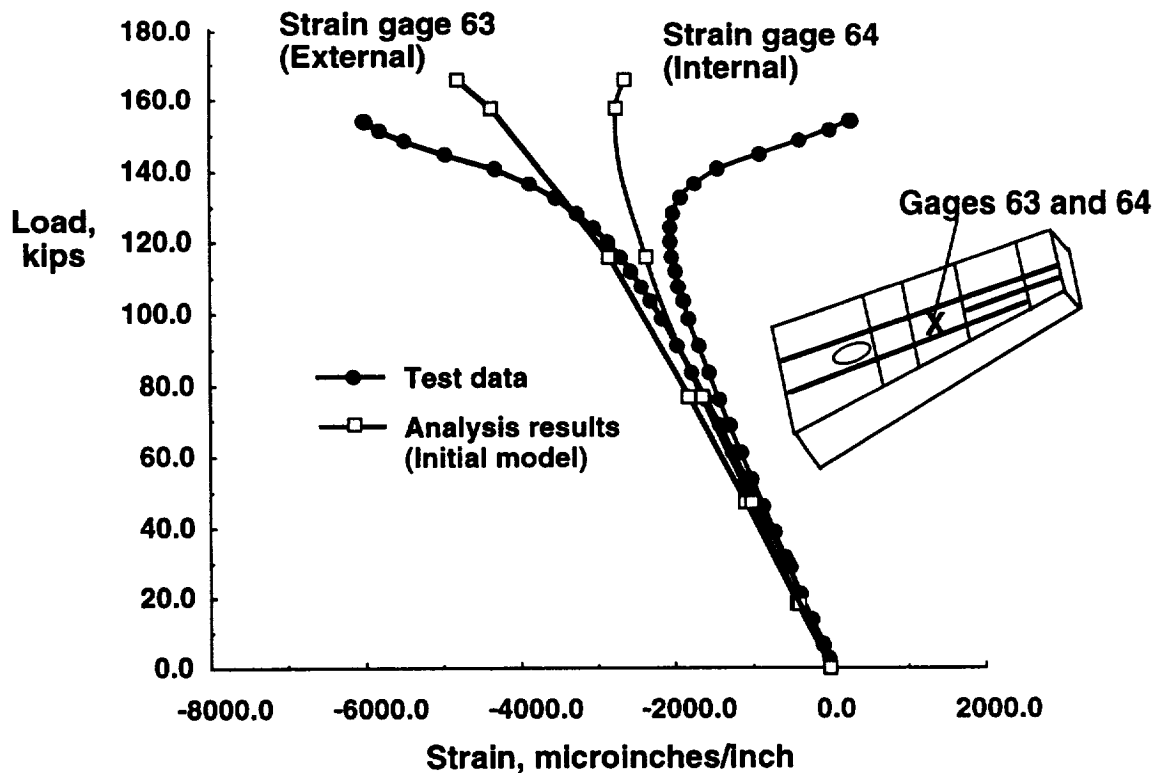
Figure 11.   Comparison of strain results from test and initial analysis for strain
gages 63 and 64.
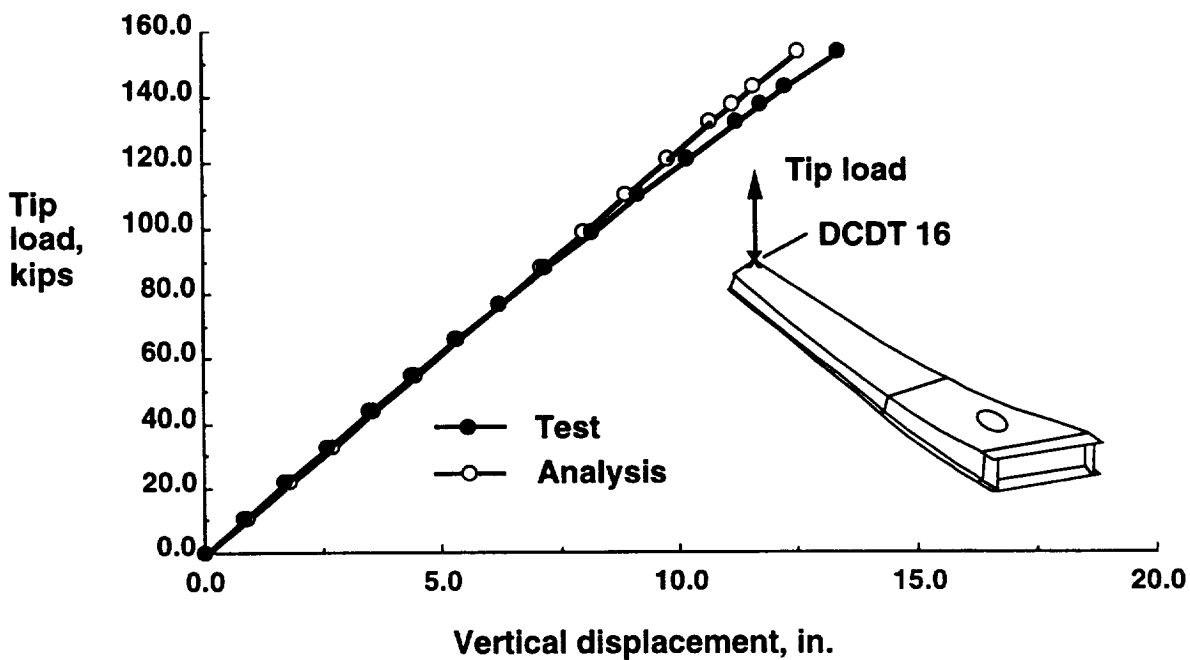
Figure 12. Stub box tip displacements for DCDT 16 at the wing tip.

20
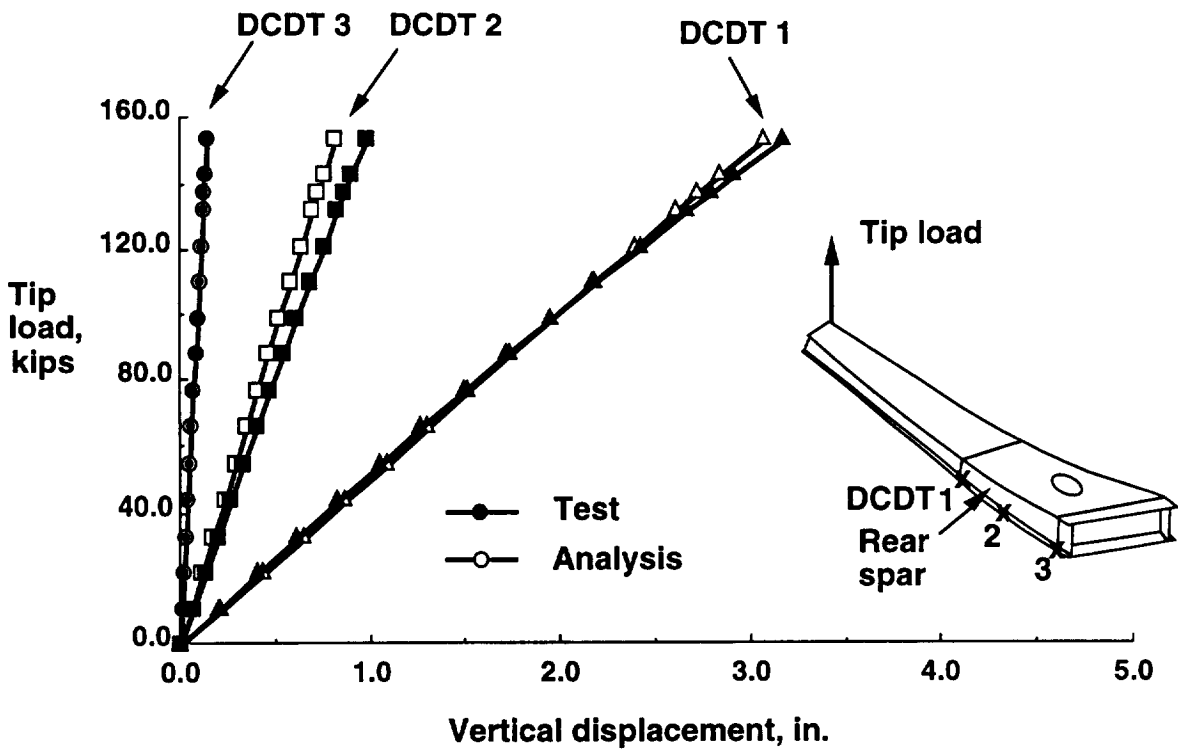
Figure 13. Vertical displacements for DCDTs 1 to 3.
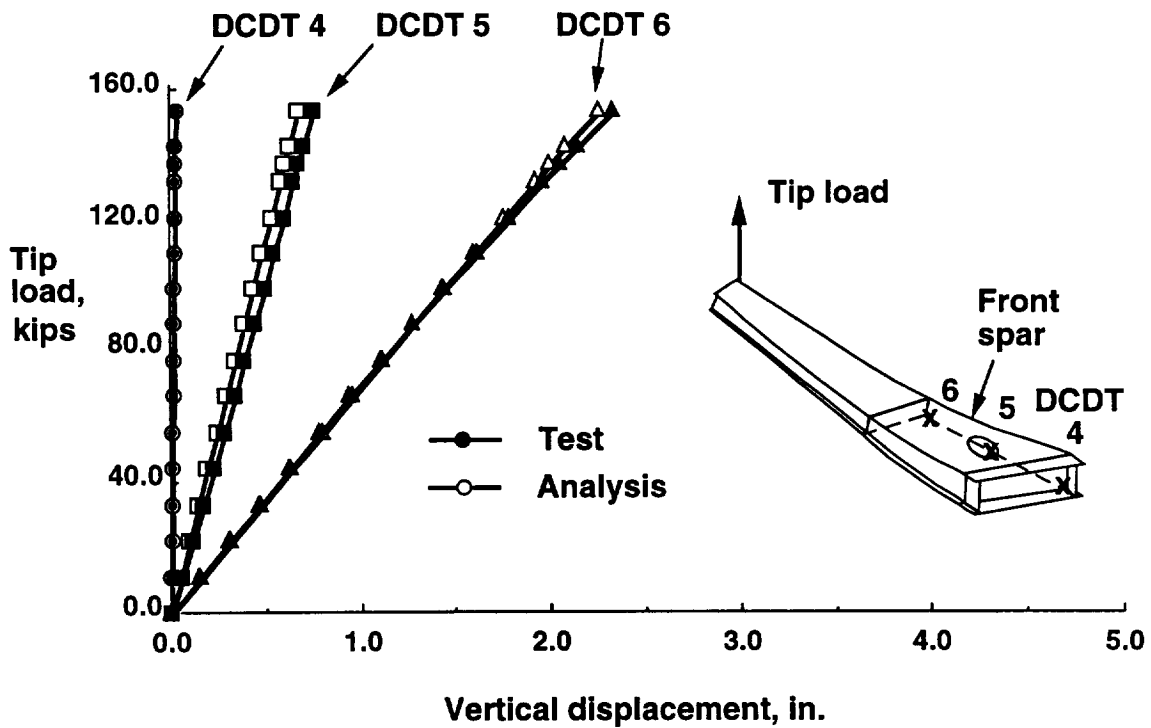
Figure 14. Vertical displacements for DCDTs 4 to 6.

Plotting scale factor = 10.0
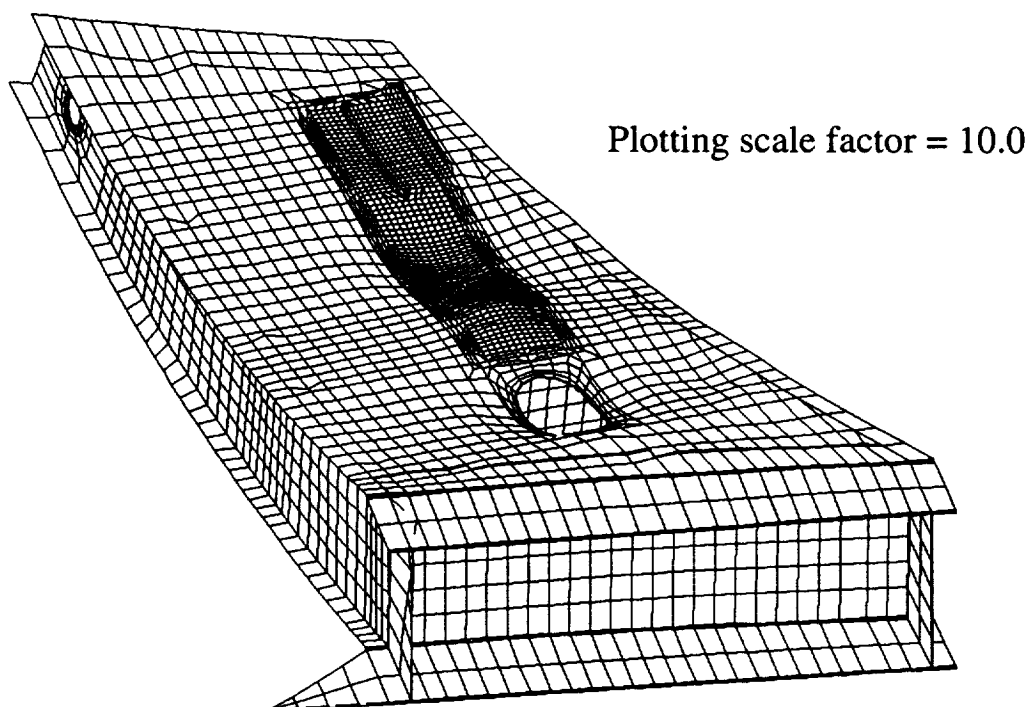
Figure 15. Deformed shape of the wing stub box at a load of 154 kips.
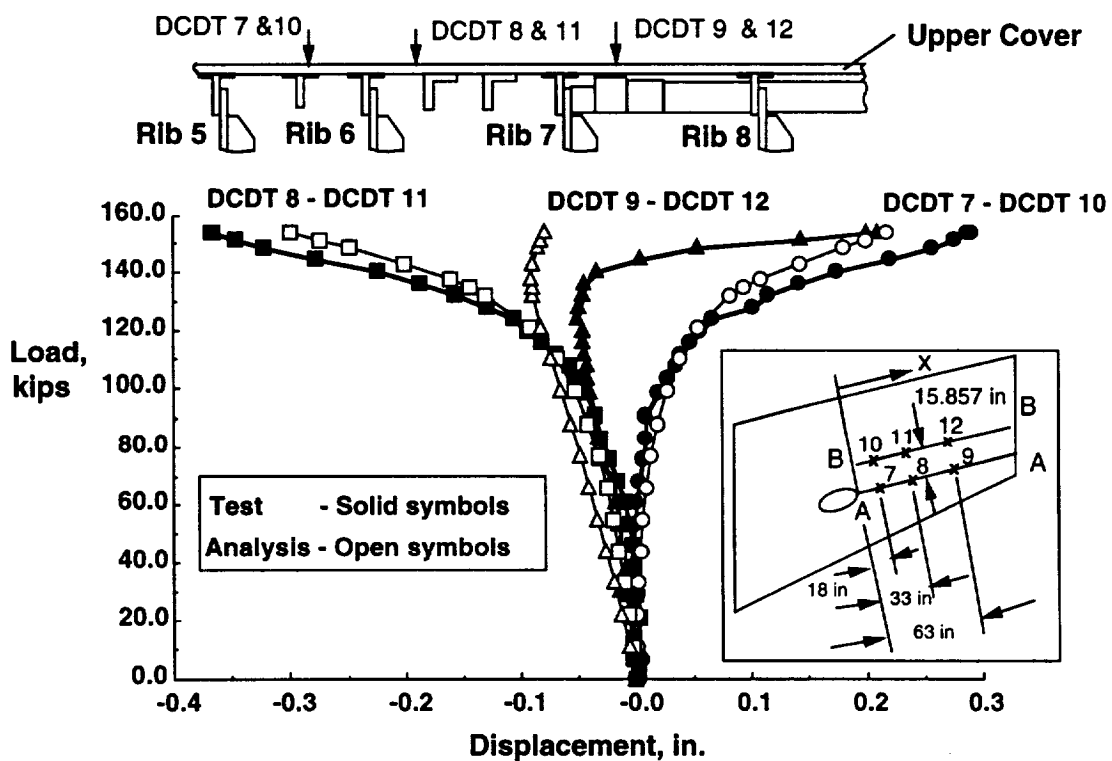
Figure 16. Relative out-of-plane displacements for DCDTs on the upper cover panel.
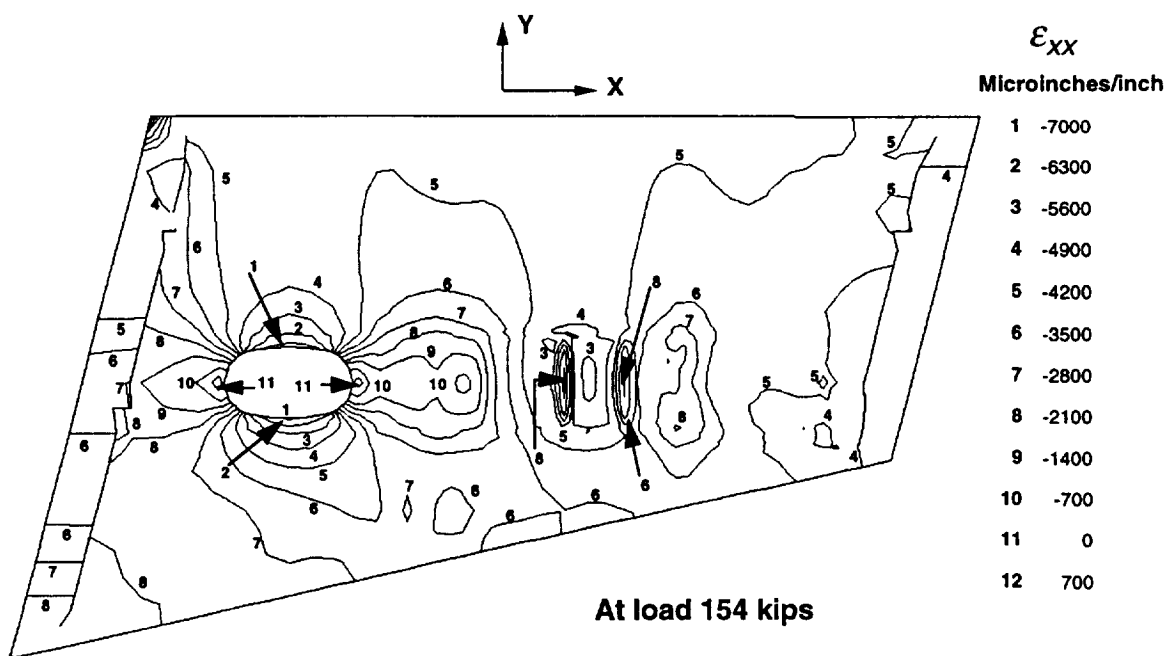
Figure 17. Axial strain contour plot for the exterior surface of the upper cover panel at the failure load.
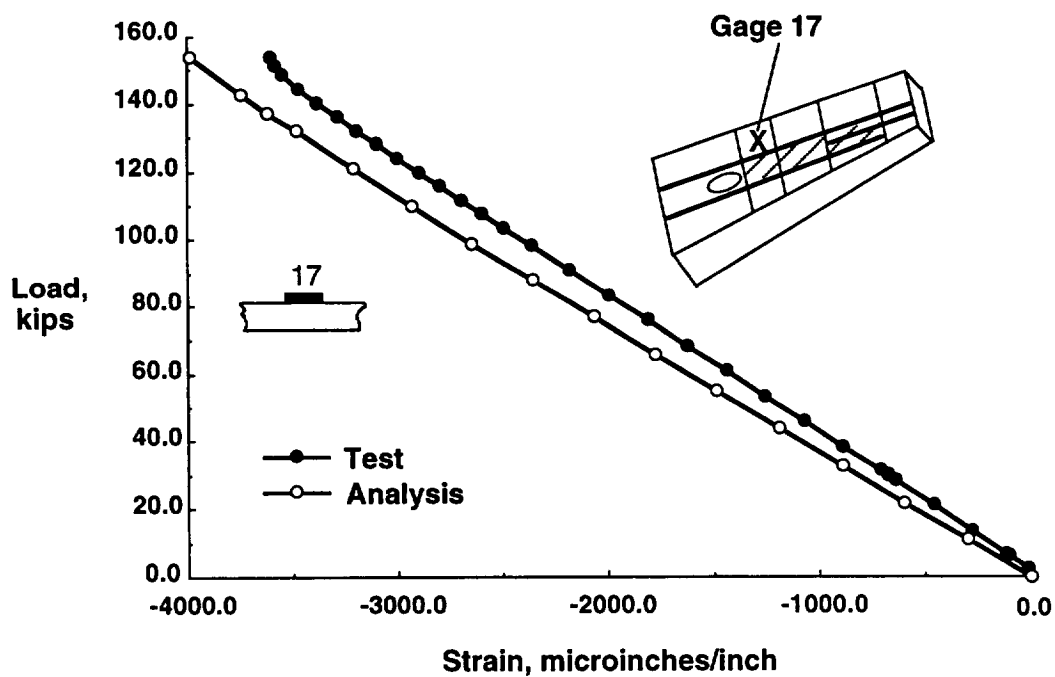
Figure 18. Correlation of far field strains for strain gage 17 on the top surface of the upper cover panel.

23
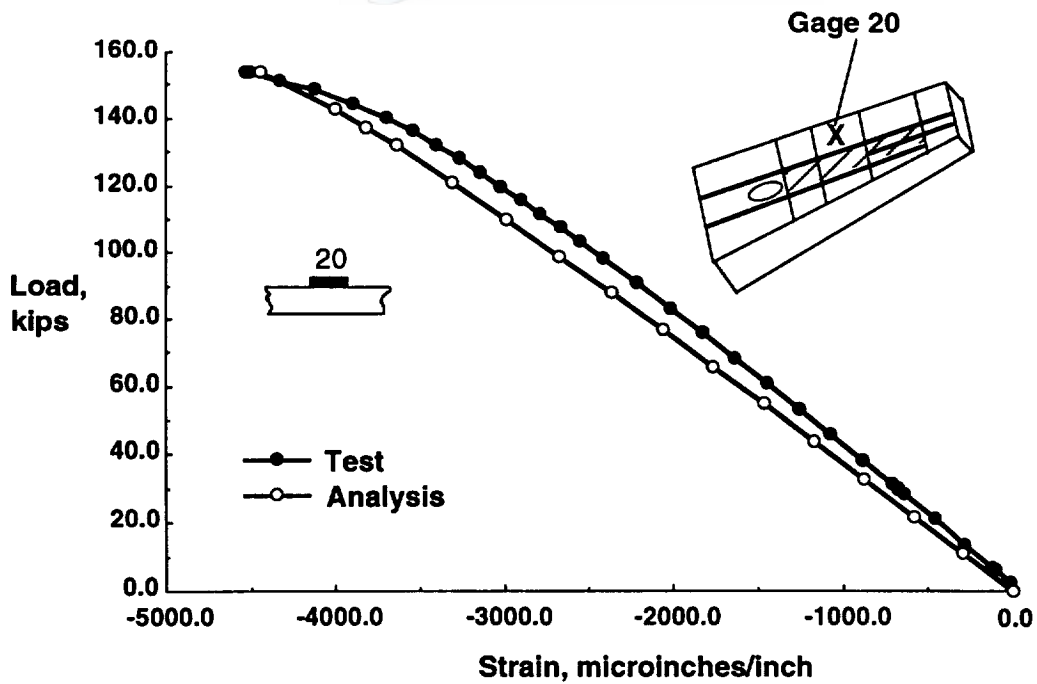
Figure 19. Correlation of far field strains for strain gage 20 on the top surface of the upper cover panel.
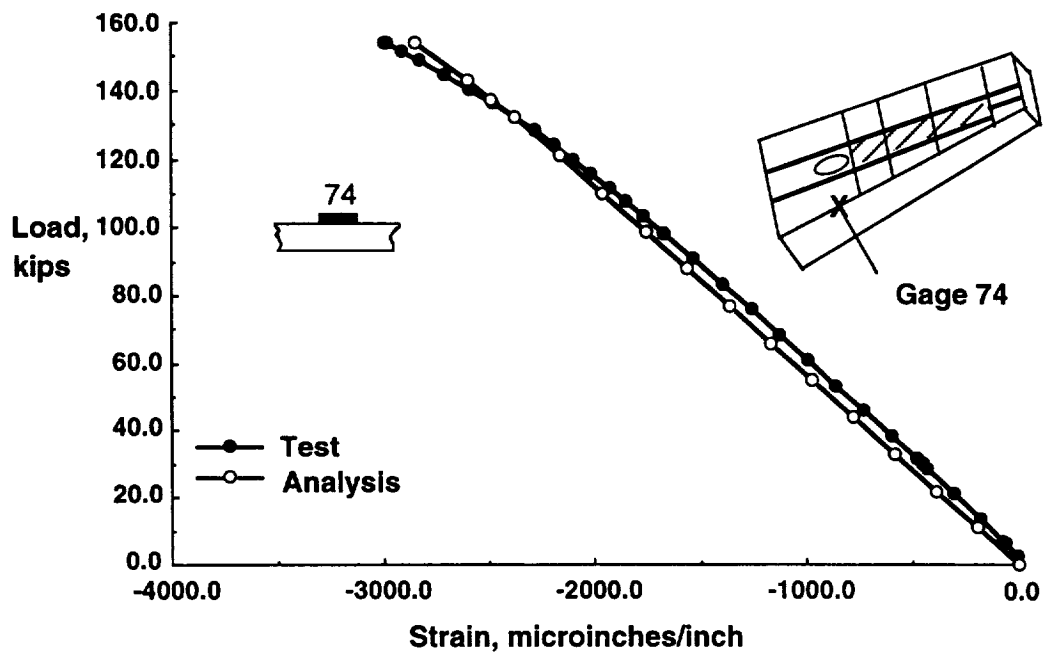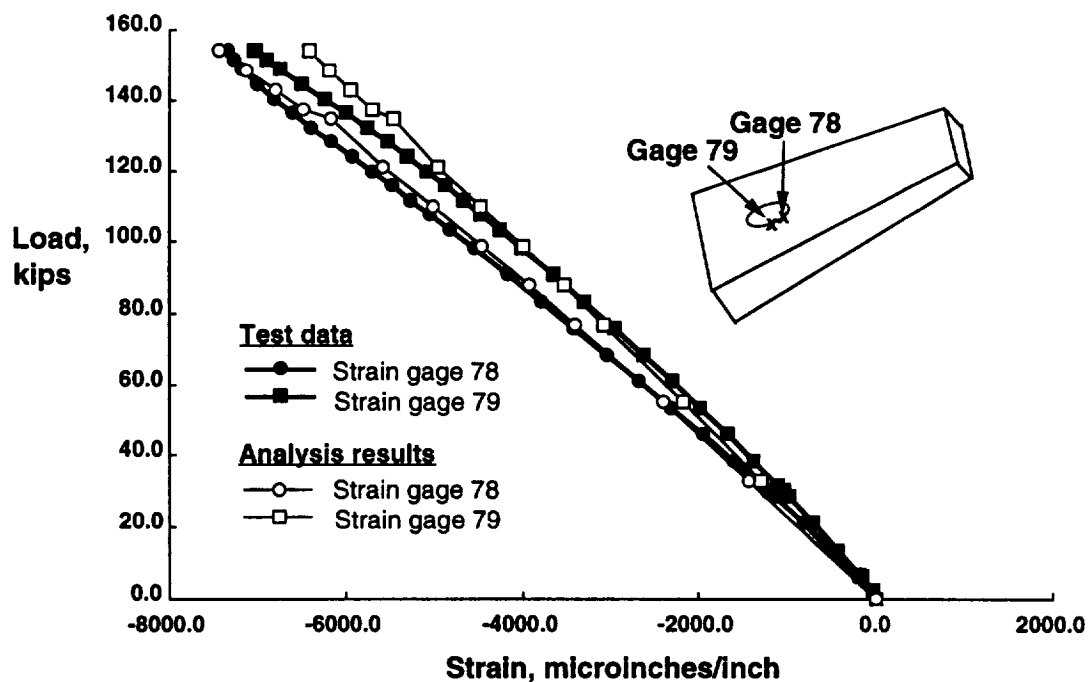

Figure 20. Correlation of far field strains for strain gage 74 on the top surface of the upper cover panel.

24
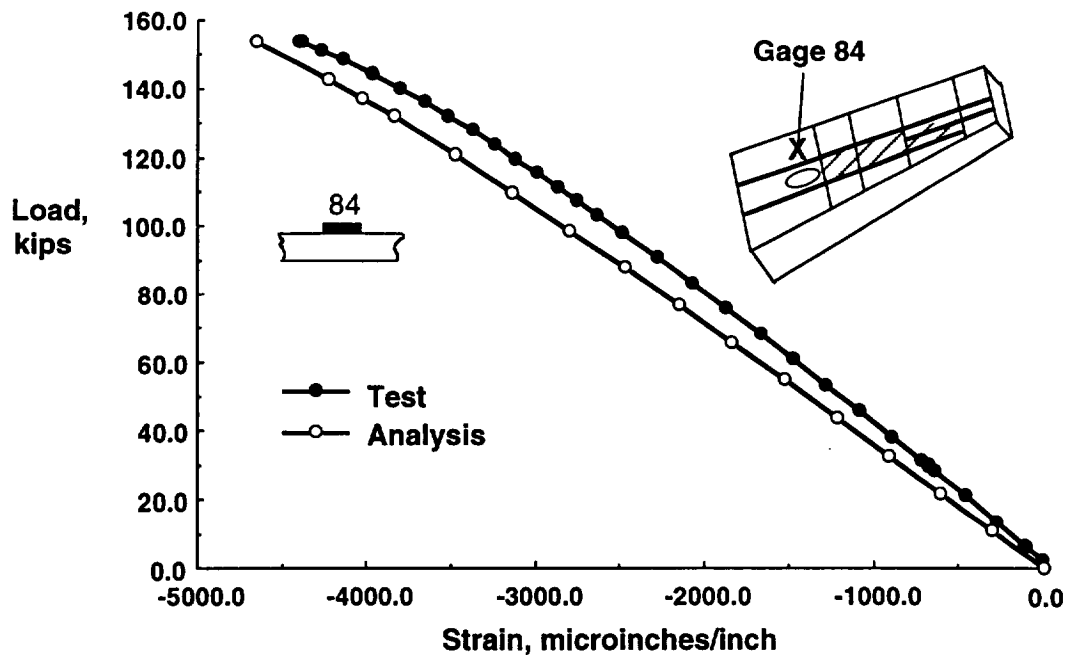
Figure 21. Correlation of far field strains for strain gage 84 on the top surface of the upper cover panel.
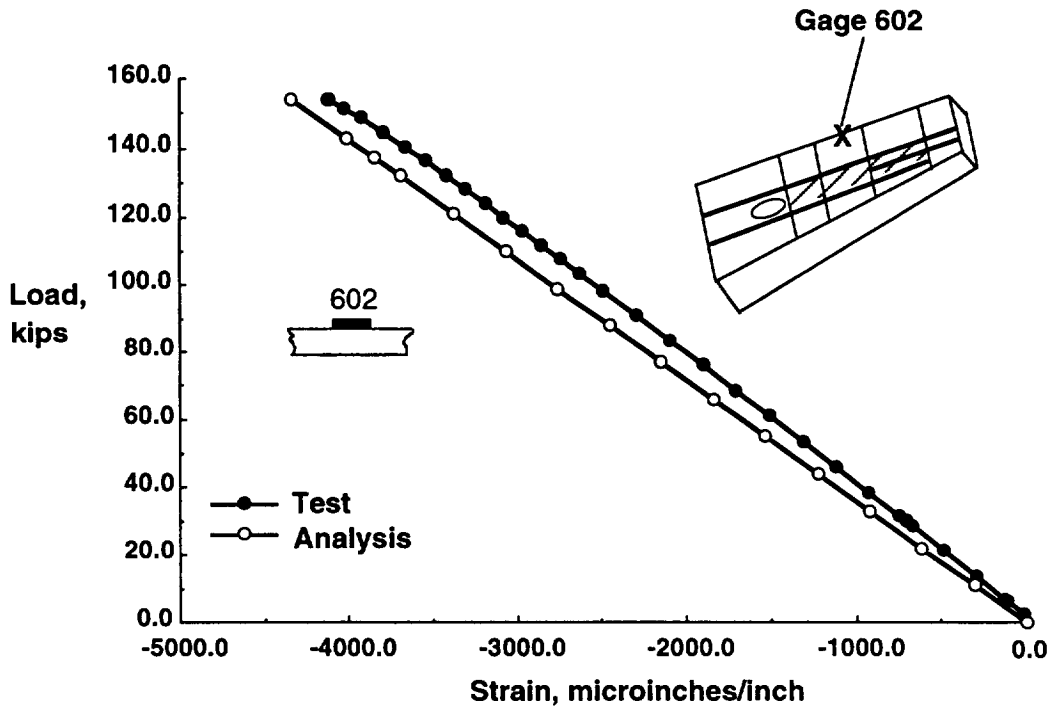
Figure 22. Correlation of far field strains for strain gage 602 on the top surface of the upper cover panel.

25

Figure 23. Correlation of strains for Gages 78 and 79.
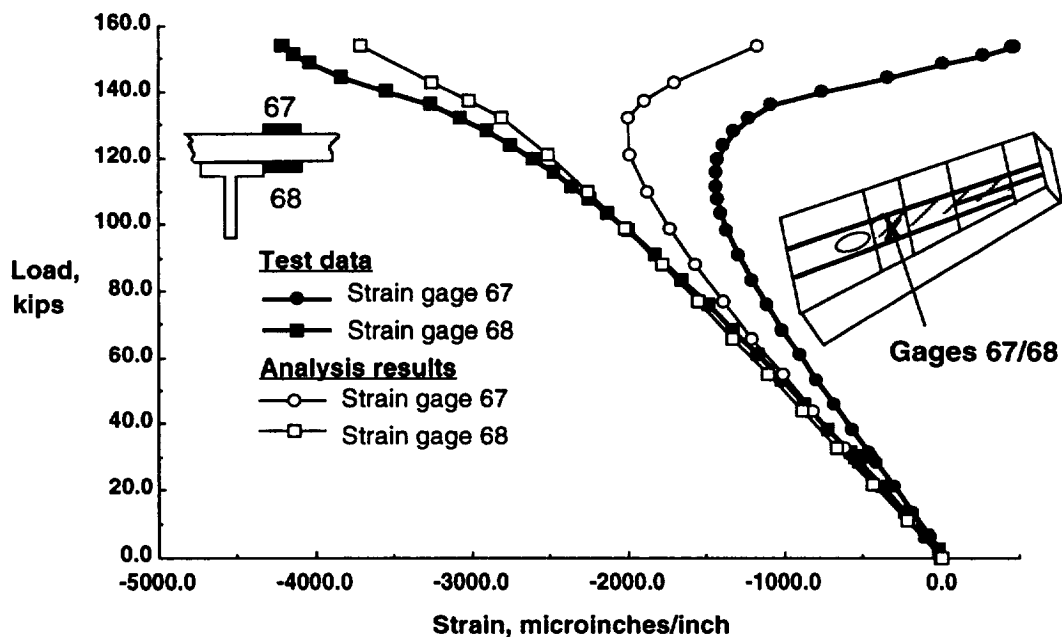
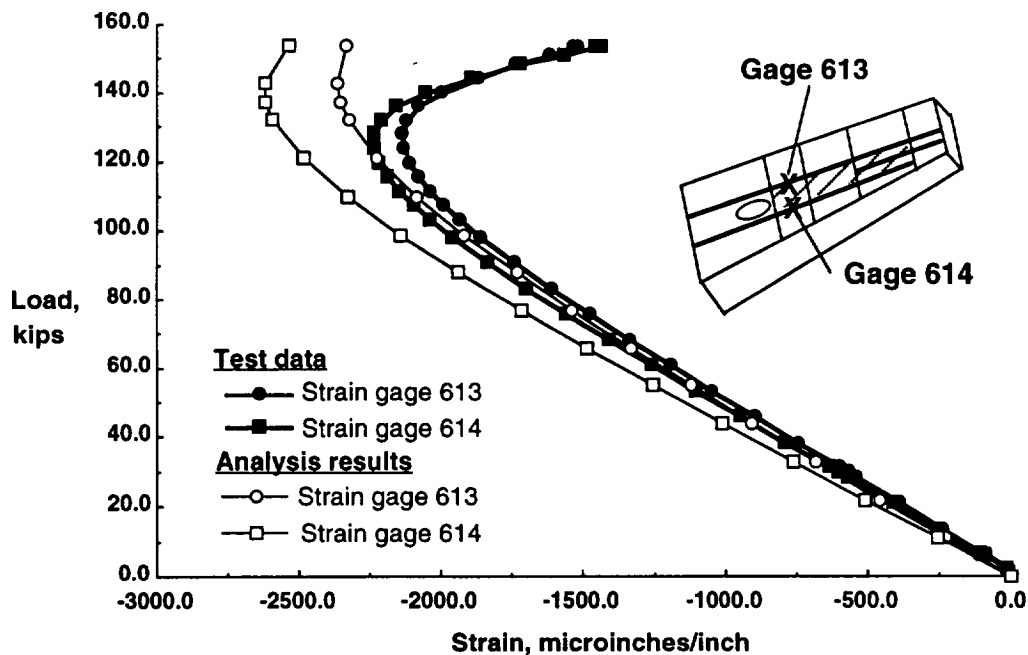Figure 24. Correlation of strains for strain gages 67 and 68.

Figure 25. Correlation of strains for strain gages 613 and 614 at the forward edge of the nonlinearly deformed region.
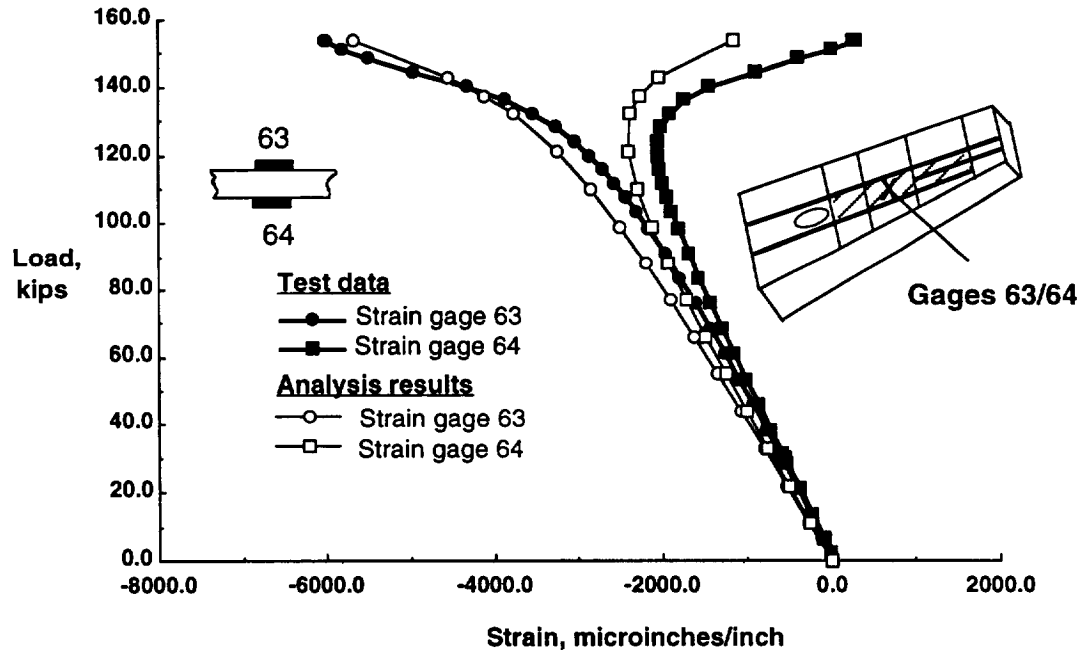

Figure 26. Correlation of strains for strain gages 63 and 64 on the upper cover panel skin.
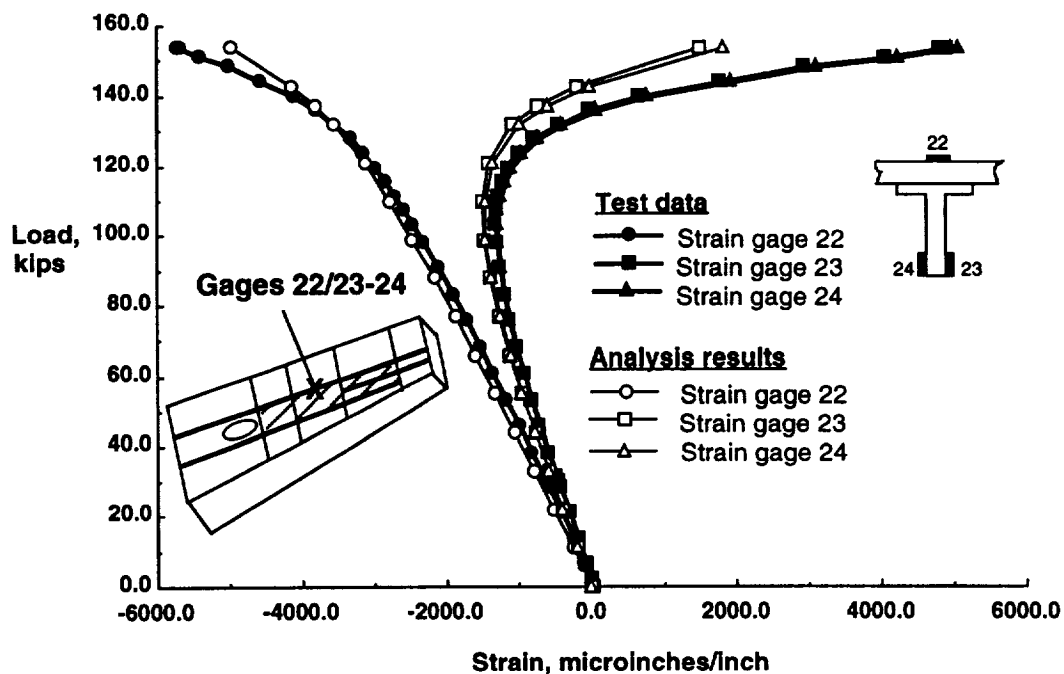
27

Figure 27. Correlation of strains for strain gages 22 , 23, and 24 at the aft edge of the highly nonlinearly deformed region.
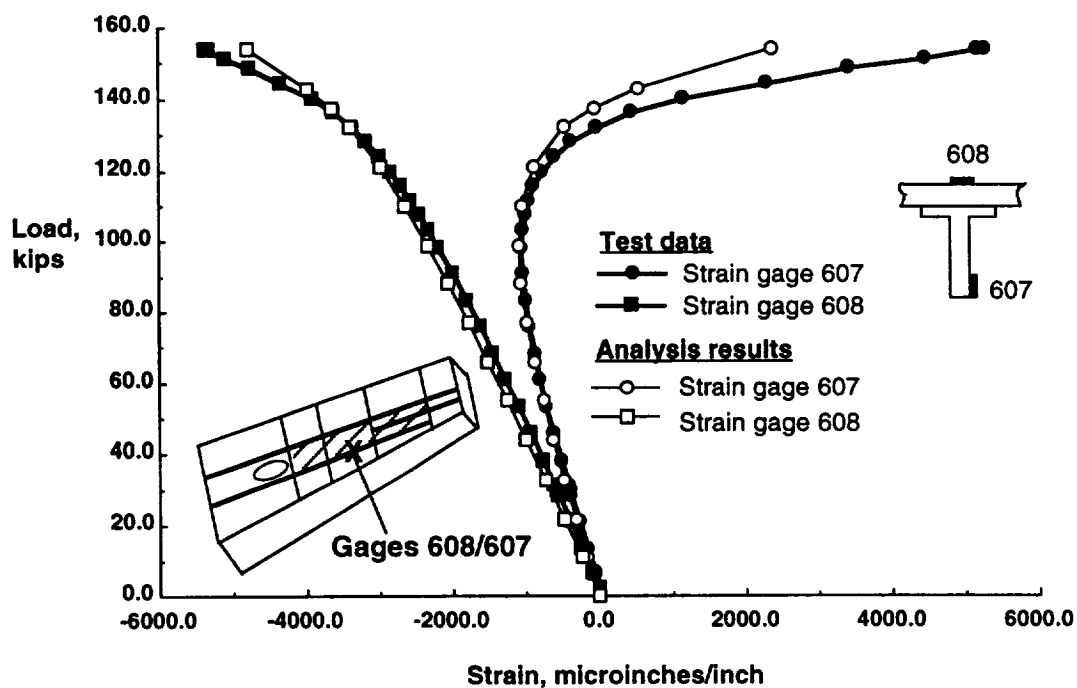
Figure 28. Correlation of strains for strain gages 607 and 608 on the forward edge of the highly nonlinearly defromed region.
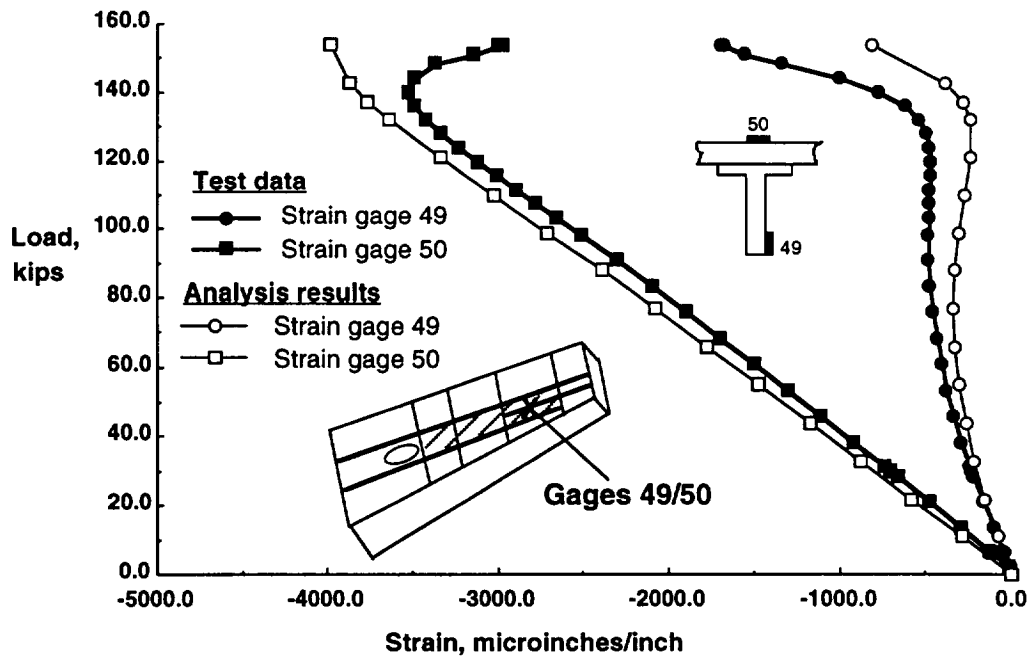
28

Figure 29. Correlation of strains for strain gages 49 and 50 on the runout stringer.
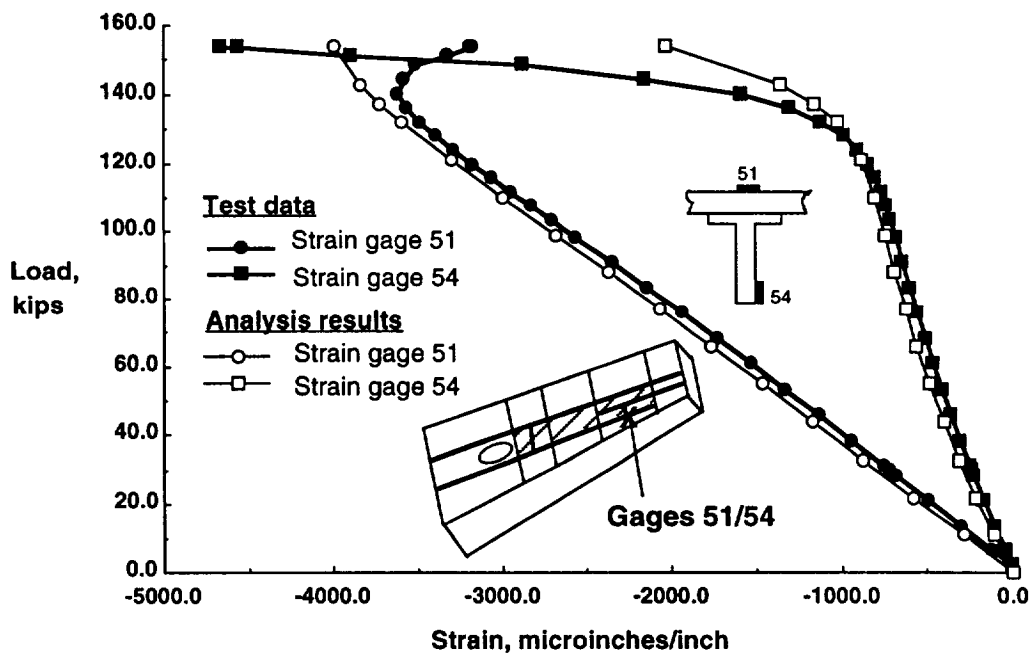

Figure 30. Correlation of strains for strain gages 51 and 54.
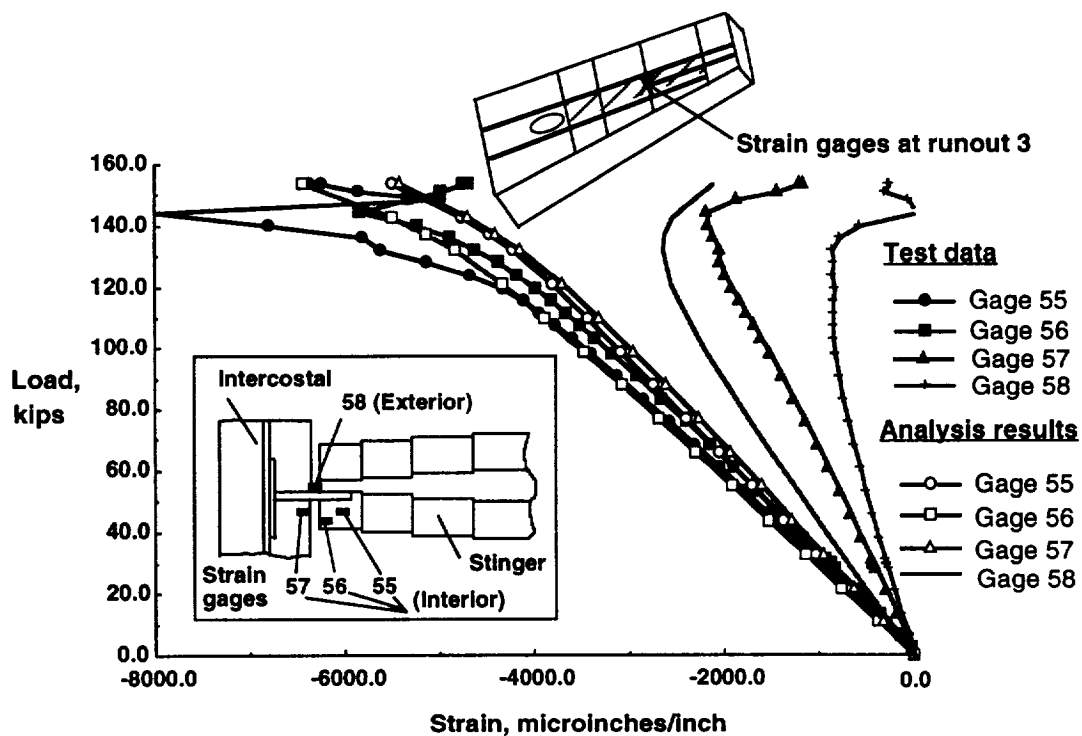
29

Figure 31. Correlation of strains for strain gages 55, 56, 57, and 58 at stringer runout 3.
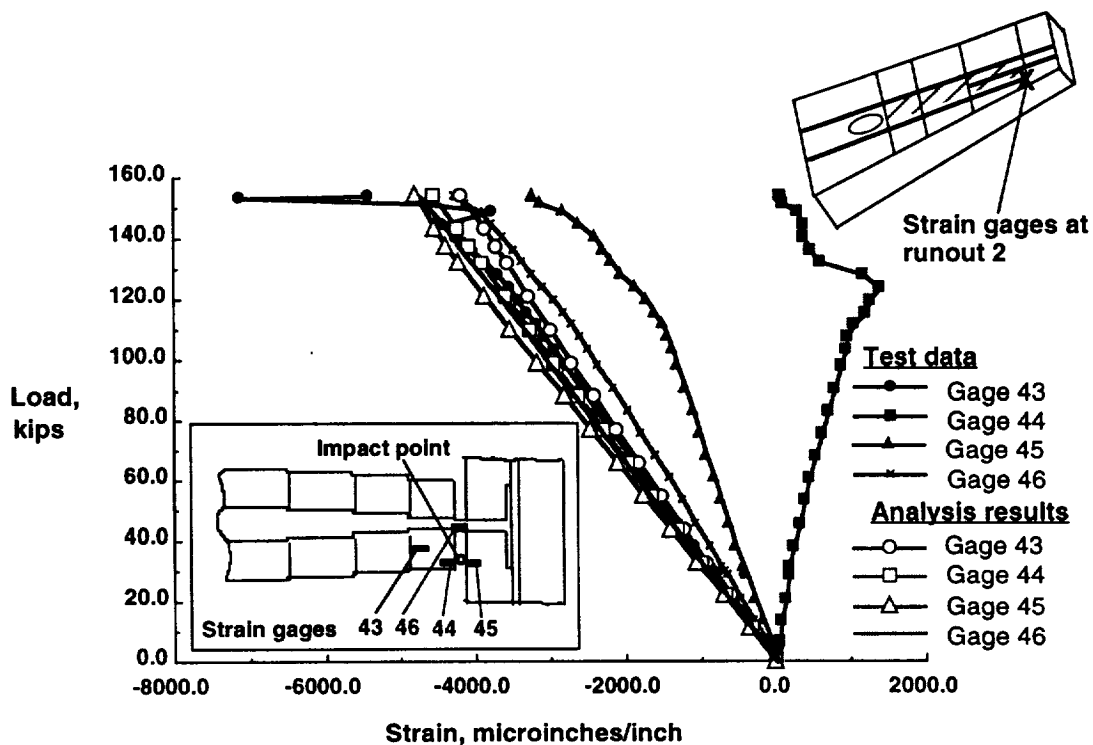

Figure 32. Correlation of strains for strain gages 43 through 46 at stringer runout 2.
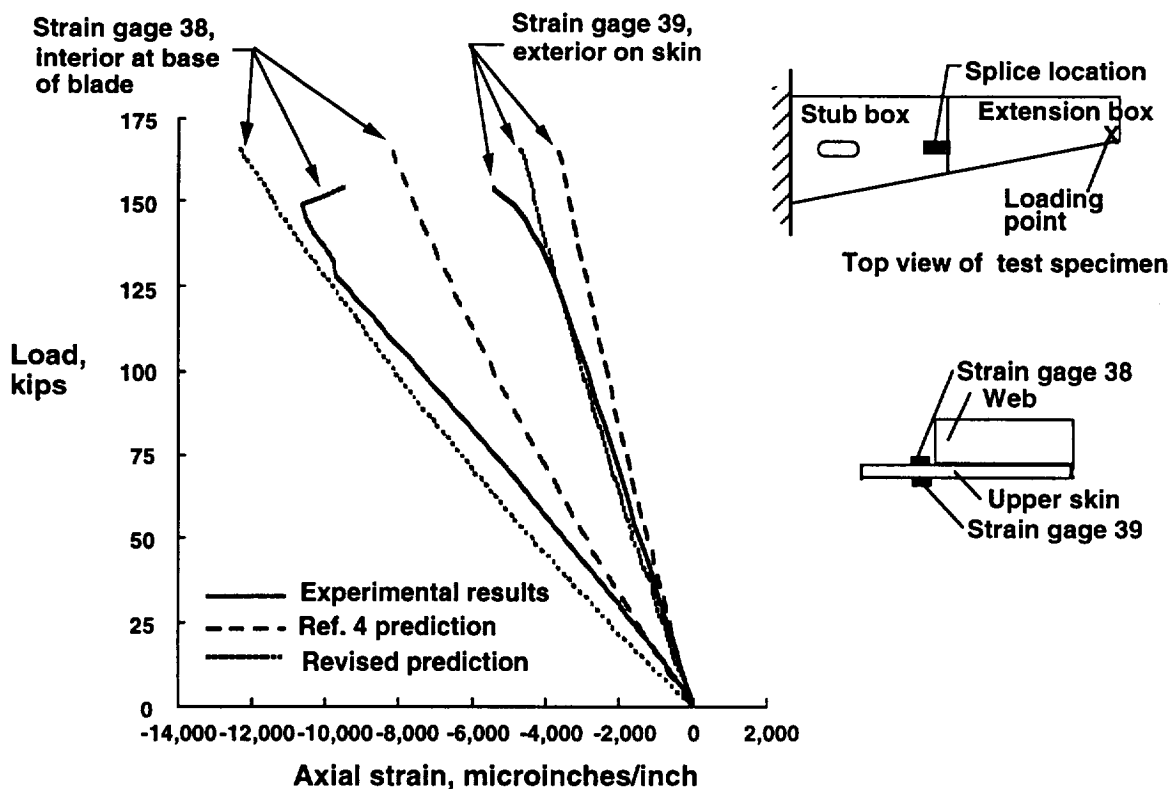
Strain gage 38, interior at base of blade

Strain gage 39, exterior on skin

Load, kips (y-axis: 0, 25, 50, 75, 100, 125, 150, 175)

Experimental results
Ref. 4 prediction
Revised prediction

Axial strain, microinches/inch (x-axis: -14,000, -12,000, -10,000, -8,000, -6,000, -4,000, -2,000, 0, 2,000)

Splice location
Stub box   Extension box
Loading point
Top view of test specimen

Strain gage 38
Web
Upper skin
Strain gage 39

Figure 33. Correlation of strains for strain gages 38 and 39 at the splice joint.

Aluminum T | Thin aluminum plate
Runout web
Intercostal
Rib
Failure line

3.25
.403
Failure
.13
.13

.5
1.825
.5
Failure

—— .075 inch thick Al plate, 1.8 inches tall
• 1/4 inch diameter bolt
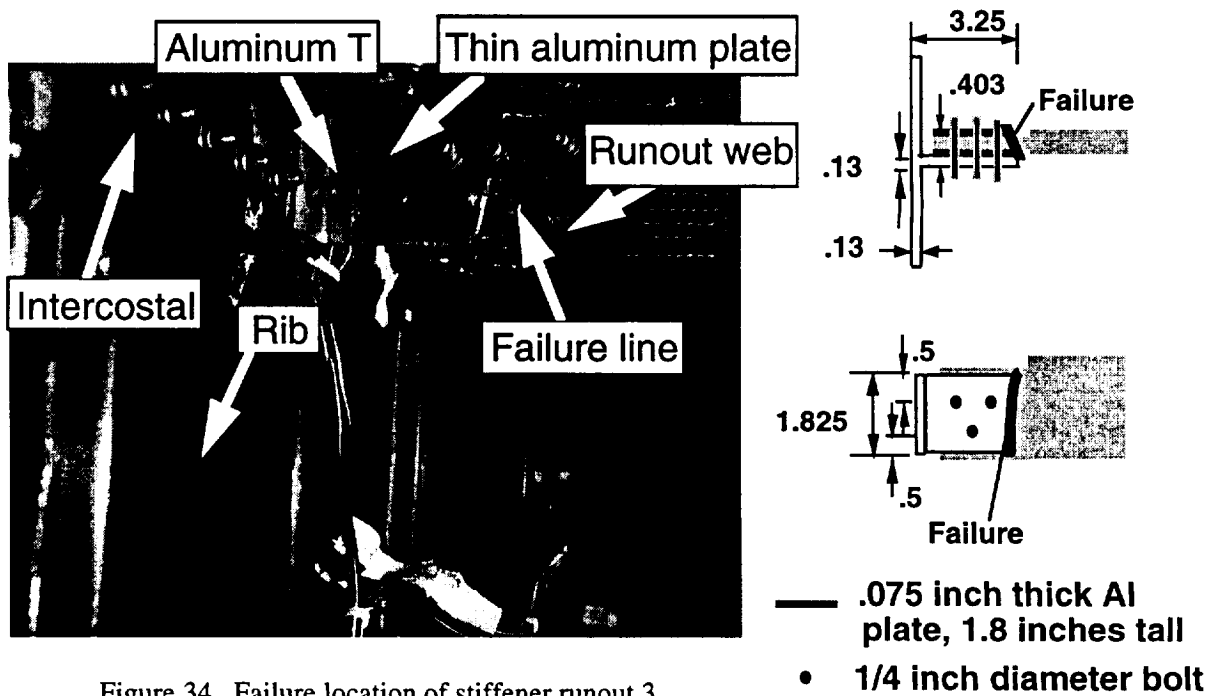
Figure 34. Failure location of stiffener runout 3.

31

ε_{XY}

Microinches/inch

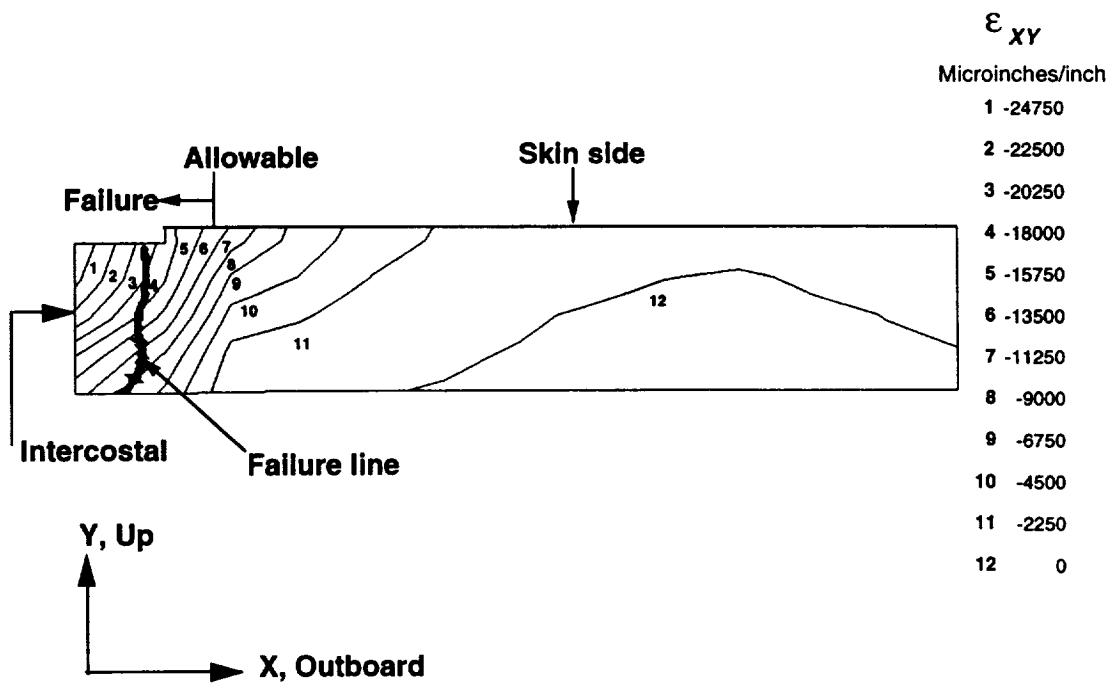|	
1	-24750
2	-22500
3	-20250
4	-18000
5	-15750
6	-13500
7	-11250
8	-9000
9	-6750
10	-4500
11	-2250
12	0

Figure 35. Shear strain contour plot for stringer runout 3 at the failure load.
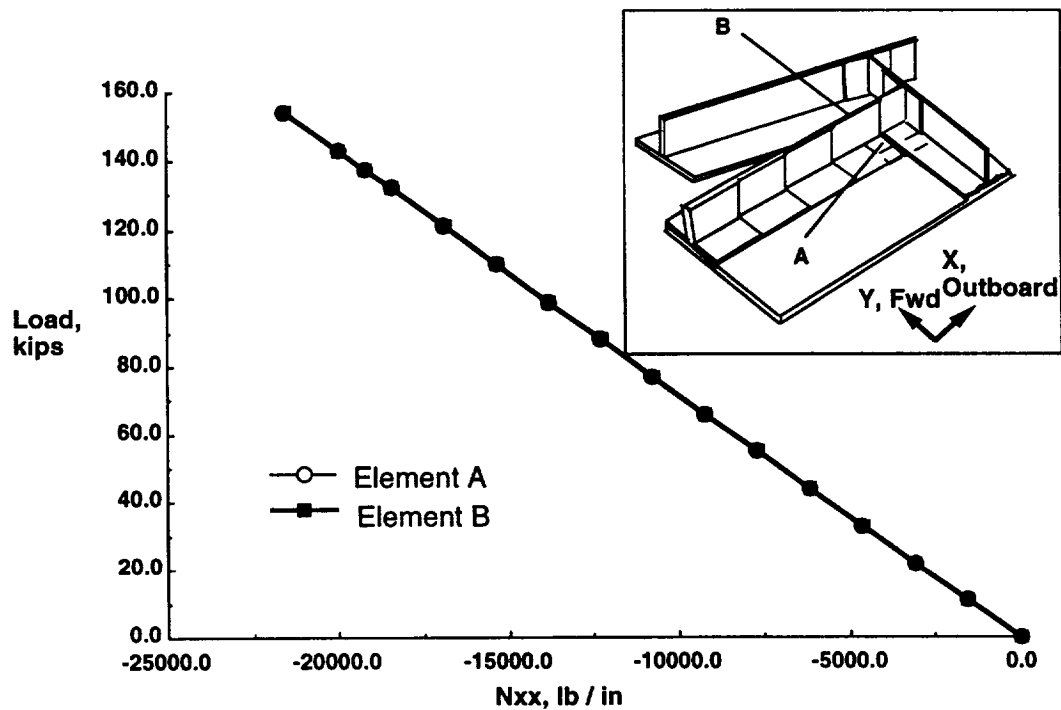
Figure 36. Axial stress resultants for elements on the stringer flange near stringer runout 2.
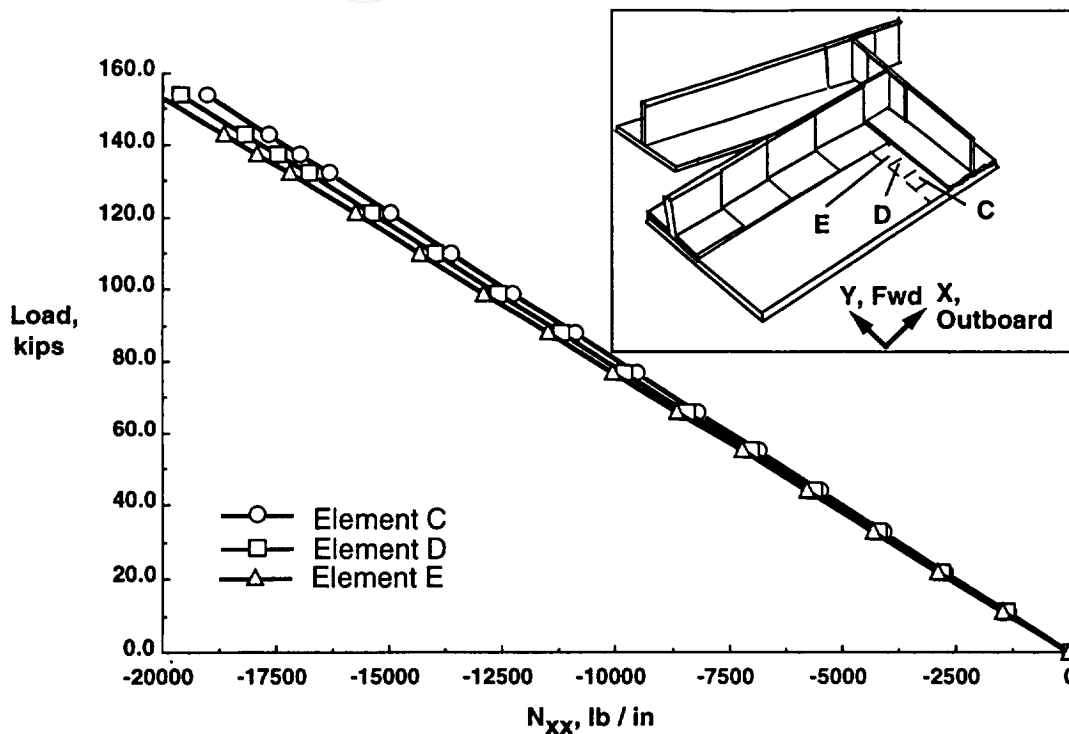
32

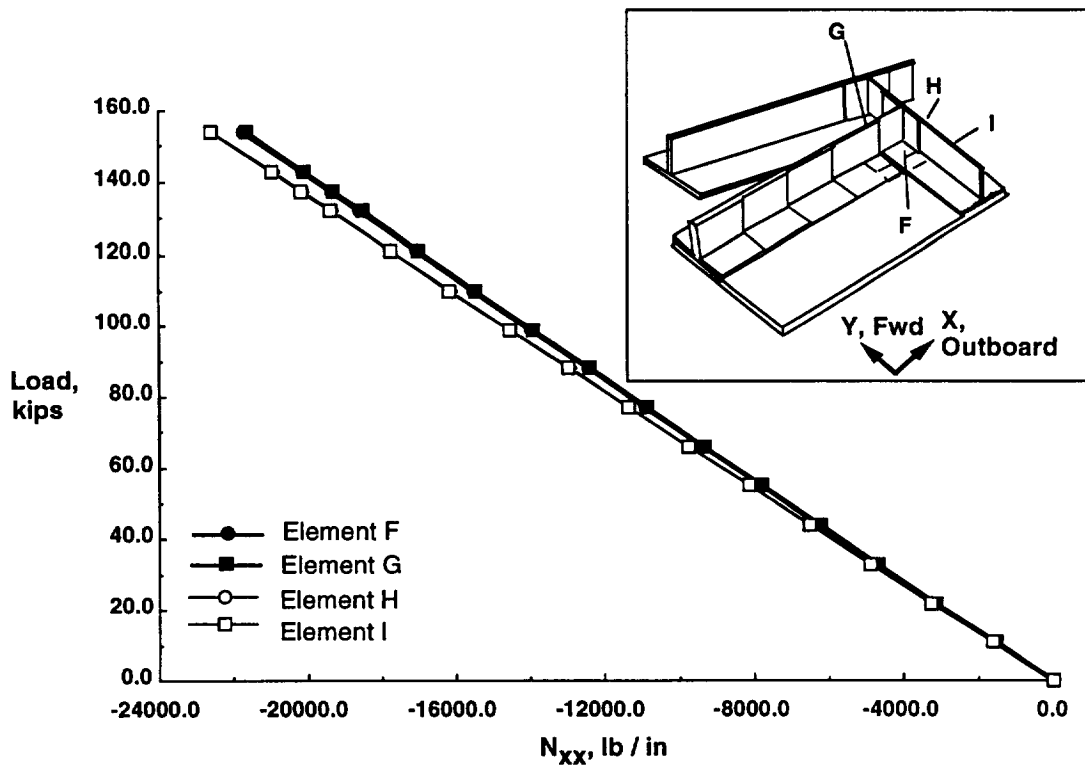Figure 37. Axial stress resultants for skin elements near stringer runout 2.

Figure 38. Axial stress resultants for elements of the intercostal flange near stringer runout 2.

33

REPORT DOCUMENTATION PAGE

Form Approved
OMB No. 0704-0188

Public reporting burden for this collection of information is estimated to average 1 hour per response, including the time for reviewing instructions, searching existing data sources, gathering and maintaining the data needed, and completing and reviewing the collection of information. Send comments regarding this burden estimate or any other aspect of this collection of information, including suggestions for reducing this burden, to Washington Headquarters Services, Directorate for Information Operations and Reports, 1215 Jefferson Davis Highway, Suite 1204, Arlington, VA 22202-4302, and to the Office of Management and Budget, Paperwork Reduction Project (0704-0188), Washington, DC 20503.

1. AGENCY USE ONLY *(Leave blank)*	2. REPORT DATE	3. REPORT TYPE AND DATES COVERED
	July 1996	Technical Memorandum

4. TITLE AND SUBTITLE	5. FUNDING NUMBERS
Correlation of Structural Analysis and Test Results for the McDonnell Douglas Stitched/RFI All-Composite Wing Stub Box	538-10-11-02

6. AUTHOR(S)

John T. Wang, Dawn C. Jegley, Harold G. Bush, and Stephen C. Hinrichs

7. PERFORMING ORGANIZATION NAME(S) AND ADDRESS(ES)	8. PERFORMING ORGANIZATION REPORT NUMBER
NASA Langley Research Center
Hampton, VA 23681-0001	

9. SPONSORING / MONITORING AGENCY NAME(S) AND ADDRESS(ES)	10. SPONSORING / MONITORING AGENCY REPORT NUMBER
National Aeronautics and Space Administration
Washington, DC 20546-0001	NASA TM-110267

11. SUPPLEMENTARY NOTES

12a. DISTRIBUTION / AVAILABILITY STATEMENT	12b. DISTRIBUTION CODE
Unclassified - Unlimited
Subject Category 39	

13. ABSTRACT *(Maximum 200 words)*

The analytical and experimental results of an all-composite wing stub box are presented in this report. The wing stub box, which is representative of an inboard portion of a commercial transport high-aspect-ratio wing, was fabricated from stitched graphite-epoxy material with a Resin Film Infusion manufacturing process. The wing stub box was designed and constructed by the McDonnell Douglas Aerospace Company as part of the NASA Advanced Composites Technology program. The test article contained metallic load-introduction structures on the inboard and outboard ends of the graphite-epoxy wing stub box. The root end of the inboard load introduction structure was attached to a vertical reaction structure, and an upward load was applied to the outermost tip of the outboard load introduction structure to induce bending of the wing stub box. A finite element model was created in which the center portion of the wing-stub-box upper cover panel was modeled with a refined mesh. The refined mesh was required to represent properly the geometrically nonlinear structural behavior of the upper cover panel and to predict accurately the strains in the stringer webs of the stiffened upper cover panel. The analytical and experimental results for deflections and strains are in good agreement.

14. SUBJECT TERMS	15. NUMBER OF PAGES
Composite Wing Box, Stitched Composites, Resin Film Infusion, Finite Element Analysis, Geometrically Nonlinear Analysis, Impact Damage, Correlation of Analysis and Test Results	34
	16. PRICE CODE
	A03

17. SECURITY CLASSIFICATION OF REPORT	18. SECURITY CLASSIFICATION OF THIS PAGE	19. SECURITY CLASSIFICATION OF ABSTRACT	20. LIMITATION OF ABSTRACT
UNCLASSIFIED	UNCLASSIFIED	UNCLASSIFIED	Unlimited

NSN 7540-01-280-5500

Standard Form 298 (Rev. 2-89)
Prescribed by ANSI Std. Z39-18
298-102